MASTERARBEIT | MASTER'S THESIS

Titel | Title

Effects of an Enterocyte-Specific Knockout of Arginase 2 on Nitric Oxide Homeostasis and Intestinal Barrier Permeability in Mice

verfasst von | submitted by

Kyra Victoria Anastopoulos

angestrebter akademischer Grad | in partial fulfilment of the requirements for the degree of

Master of Science (MSc)

Wien | Vienna, 2026

Studienkennzahl lt. Studienblatt | Degree programme code as it appears on the student record sheet:	UA 066 865
Studienrichtung lt. Studienblatt | Degree programme as it appears on the student record sheet:	Masterstudium Molecular Biology
Betreut von | Supervisor:	Univ.-Prof. Dipl. oec. troph. Dr. Ina Bergheim Privatdoz.

Acknowledgements

I would like to begin by expressing my sincere gratitude to Univ.-Prof. Dipl. oec. troph. Dr. Ina Bergheim, for the opportunity to join her research group and for her continuous guidance throughout my master's thesis. I am deeply appreciative of her kindness, encouragement, and invaluable insight. Vielen Dank!

My special thanks go to Dr. Anja Baumann for her remarkable patience and steadfast support. I am truly thankful for the time and dedication she invested in teaching me, addressing my many questions, and guiding the development of this thesis. Vielen lieben Dank!

I would also like to extend my appreciation to the researchers and PhD students in our group—Dr. Annette Brandt, Dr. Katharina Burger, and Katja Csarmann—for their readiness to share their knowledge and expertise. I am equally grateful to the other members of the Bergheim group, Beate and Spela, for maintaining the laboratory, introducing me to new experimental techniques, caring for the animals, and for the many enjoyable conversations along the way. Danke!

I am thankful for my lab colleagues and fellow master's students. Thank you all for making every day in the lab interesting and for the great camaraderie. I would like to acknowledge Anna-Christina and Alessio for their friendship both inside and outside the lab, their collaboration, support, and encouragement. Tausend Dank!

Finally, my deepest gratitude goes to my family for their unwavering belief in me and their unconditional love and support throughout my many endeavors. I am also deeply grateful to my best friend, Sierra Jane, and my partner, Jan, whose constant reassurance, patience, and encouragement carried me through this journey. This master's degree would not have happened without you all. Thank you from the bottom of my heart.

Abstract

With the increasing prevalence of intestinal barrier–related diseases, understanding the mechanisms regulating epithelial integrity is of growing importance. Arginase 2 (Arg2) is a mitochondrial enzyme that regulates inducible nitric oxide synthase (iNOS) through competition for substrate L-arginine. iNOS-derived nitric oxide (NO) is a crucial mediator of intestinal barrier dysfunction and has been linked to the development of diseases related to leaky gut. Previous studies have shown that reduced arginase activity in small-intestinal tissue is linked to alterations in NO homeostasis and impaired barrier function. To better understand this link, this study investigated an enterocyte-specific Arg2 knockout mouse model.

In male Arg2 knockout and wild-type animals aged 3-5 months, arginase activity was measured in small-intestinal tissue, and Arg2 and occludin protein levels were analyzed by Western blot and immunohistochemistry. Nitrite concentration, an indicator of NO synthesis, was measured using the Griess assay. Intestinal permeability of the small and large intestines was assessed using an ex vivo everted gut-sac model and a xylose permeability assay. Liver histology was evaluated by hematoxylin and eosin staining, and NAFLD activity scoring, and liver triglyceride levels were quantified.

Our data suggest that the enterocyte-specific Arg2 knockout in mice is associated with alterations of tight-junction protein occludin in small-intestinal tissue, increased intestinal permeability in the large intestine, signs of liver inflammation, and no significant changes in nitrite levels in small-intestinal tissue. Further studies are needed to explore the molecular mechanisms of this knockout's effects, its role in NO homeostasis, and implications for human health.

Abstract – German

Mit der zunehmenden Prävalenz von Erkrankungen, die mit einer Störung der intestinalen Barriere assoziiert sind, gewinnt das Verständnis der Mechanismen zur Regulation der epithelialen Integrität zunehmend an Bedeutung. Arginase 2 (Arg2) ist ein mitochondriales Enzym, das die Aktivität der induzierbaren Stickstoffmonoxid-Synthase (iNOS) durch Konkurrenz um das Substrat L-Arginin reguliert. Das von iNOS gebildete Stickstoffmonoxid (NO) gilt als zentraler Mediator der intestinalen Barrieredysfunktion und wird mit der Entstehung von Erkrankungen im Zusammenhang mit einem „Leaky Gut“ in Verbindung gebracht. Frühere Studien zeigten, dass eine verminderte Arginaseaktivität im Dünndarm mit Veränderungen der NO-Homöostase und einer beeinträchtigten Barrierefunktion assoziiert ist.

Zur weiteren Untersuchung dieses Zusammenhangs wurde in der vorliegenden Studie ein enterozytenspezifisches Arg2-Knockout-Mausmodell analysiert. In männlichen Arg2-Knockout- und Wildtyp-Tieren im Alter von 3–5 Monaten wurde die Arginaseaktivität im Dünndarm bestimmt. Zusätzlich wurden die Proteinexpression von Arg2 und Occludin mittels Western Blot und Immunhistochemie analysiert. Die Nitritkonzentration als Indikator für die NO-Synthese mit dem Griess-Assay gemessen. Die intestinale Permeabilität des Dünn- und Dickdarms wurde mithilfe eines ex vivo Everted-Gut-Sac-Modells sowie eines Xylose-Permeabilitätsassays bestimmt. Zudem wurden Leberhistologie, NAFLD-Aktivitätsscore und hepatische Triglyzeridspiegel analysiert.

Die Ergebnisse deuten darauf hin, dass die enterozytenspezifische Deletion von Arg2 in Mäusen mit Veränderungen des Tight-Junction-Proteins Occludin im Dünndarm, erhöhter Permeabilität im Dickdarm sowie Anzeichen einer Leberentzündung assoziiert ist, während keine signifikanten Veränderungen der Nitritkonzentrationen im Dünndarm festgestellt wurden. Weitere Studien sind erforderlich, um die zugrunde liegenden molekularen Mechanismen und mögliche Relevanz für die menschliche Gesundheit zu klären.

Table of Contents

List of Figures

List of Tables

List of Abbreviations

APS	Ammonium Peroxydisulfate
Arg1	Arginase 1
Arg2	Arginase 2
ASL	Argininosuccinate lyase
ASS	Argininosuccinate synthetase
BSA	Bovine Serum Albumin
$CaCl_2*2H_2O$	Calcium chloride dihydrate
CAT	Cationic amino acid transporter
DAB	3,3'-Diaminobenzidine
DBPS	Dulbecco's Phosphate Buffered Saline
ddH_2O	Double distilled water
dH_2O	Distilled water
DMEM	Dulbecco's Modified Eagle Medium
DTT	DL-Dithiothreitol
EtOH	Ethanol
g	Gram
GI	Gastrointestinal
H. pylori	Helicobacter pylori
H&E	Hematoxylin and Eosin
H_2SO_4	Sulphuric Acid
H_3PO_4	Ortho-phosphoaisc acid
HCL	Hydrochloric Acid
hr/s	Hour/s
HRP	Horseradish Peroxidase
IBD	Irritable Bowel Disease
IECs	Intestinal epithelial cells
iNOS	Inducible Nitric Oxide Synthase
KCL	Potassium chloride
KH_2PO_4	Potassium dihydrogen phosphate
KO or -/-	Knockout
KRH	Krebs-Henseleit-bicarbonate buffer (0.2% bovine serum albumin)
L-Arg	L - Arginine
LP	Lamina propria
MASLD	Metabolic dysfunction–associated steatotic liver disease
$MgSO_4$	Magnesium sulfate
Min/s	Minute/s
$MnCl_2*4H_2O$	Manganese (II) Chloride Tetrahydrate
mRNA	Messenger RNA

mTOR	Mechanistic target of rapamycin
Na_2HPO_4	Disodium hydrogen phosphate
NaCl	Sodium chloride
$NADP^+$	Nicotinamide Adenine Dinucleotide Phosphate
NADPH	Nicotinamide Adenine Dinucleotide Phosphate (reduced)
NAFLD	Non-Alcoholic Fatty Liver Disease
NaOH	Sodium Hydroxide
NAS	NAFLD Activity Score
NFM	Nonfat Dried Milk Powder
NO	Nitric Oxide
NOS	Nitric Oxide Synthase
NOX	NADPH Oxidase
OAT	Ornithine Aminotransferase
Occ.	Occludin
ODC	Ornithine Decarboxylase
$ONOO^-$	Peroxynitrite
PA	Primary Antibody
PBS	Phosphate Buffered Saline
PVDF	Polyvinylidene Difluoride
RNS	Reactive Nitrogen species
ROS	Reactive Oxygen Species
RT	Room Temperature
SA	Secondary Antibody
SDS	Sodium Dodecyl Sulfate
SDS PAGE	Sodium Dodecyl Sulfate–Polyacrylamide Gel Electrophoresis
SEM	Standard Error of the Mean
SPF	Specific pathogen free
TBS	Tris Buffered Saline
TBST	Tris Buffered Saline with Tween 20
TEMED	Tetraacetylethylenediamine
TJ	Tight Junction
TRIS - HCL	Tris-Hydrochloride
TRIS (base)	Tris-(hydroxymethyl)-aminomethane
UK	United Kingdom
USA	United States of America
WT	Wild Type
α -ISPF	α – isonitrosopropiophenone

1. Introduction

1.1 The intestinal barrier: structure of the small and large intestine

The gastrointestinal (GI) tract is the longest component of the digestive system and constitutes the largest mucosal interface between the body and the external environment [1]. Through this extensive surface, the GI tract functions to digest and absorb nutrients, produce digestive secretions, and perform endocrine functions [1–3]. Furthermore, it is exposed to a heavy load of microbial and dietary antigens and thus serves as a crucial site for innate and adaptive immune regulation in the human body, with a renewal rate of 3-5 days [4–6].

Following the stomach, the intestinal tract consists of the small intestine, which includes the duodenum, jejunum, and ileum, and the large intestine, which comprises the cecum and colon [3]. The liver, gallbladder, and pancreas are primary accessory organs that produce and deliver secretions and enzymes to aid digestion [7]. The small intestine is the primary site for chemical digestion and nutrient absorption, accounting for approximately 90% of food breakdown [8]. The large intestine absorbs residual water, electrolytes, and other essential nutrients while trillions of microbes break down undigested material. It then facilitates fecal elimination [7,8].

All sections of the GI tract's barrier can be divided into four layers that are joined by connective tissues and vascular elements. These layers are the mucosa, submucosa, muscularis propria, and the serosa [2]. The following work describes key morphological and functional components of the small and large intestine, with a specific focus on the surface layer. The mucosa represents the innermost layer, characterized by its structural and functional complexity. It comprises the mucus layer, intestinal epithelial cells (IECs), lamina propria (LP), and the muscularis mucosae [1,3,6].

The luminal surface of the small intestine is lined by a simple columnar epithelium. The epithelium forms outward projections called villi, which maximize the absorptive surface area of the small intestine while inward invaginations, called

crypts of Lieberkühn, house stem and Paneth cells, which are essential for epithelial renewal and innate defense [2,3,5,9]. IECs are also lined with intraluminal villi, called microvilli, which further increase the surface area to enhance absorption [3]. Cell lineages that make up the intestinal epithelium include differentiated cells, Paneth cells, and stem cells. The proliferating progenitor compartment also plays a role in the cell lineages that make up the epithelium [2]. The differentiated cells of the intestine include enterocytes, enteroendocrine cells, goblet cells, tuft cells, Paneth cells, and microfold (M) cells [10].

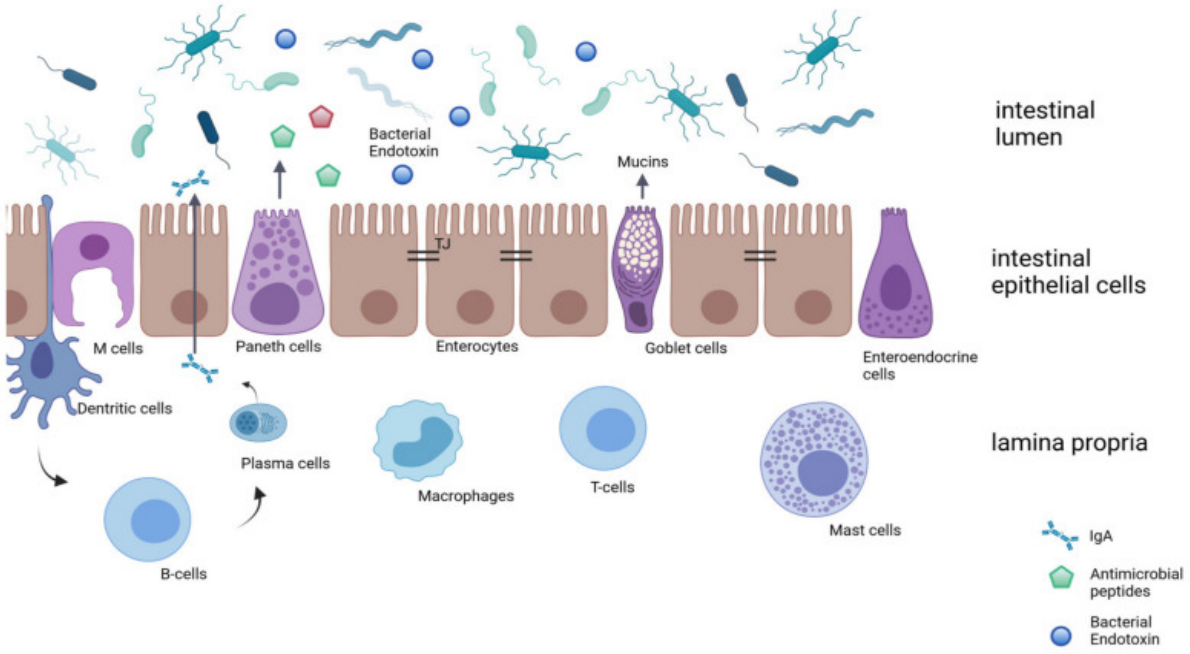

Figure 1: Schematic overview of the intestinal barrier and its key components. *The intestinal barrier includes microbial, biochemical, physical, and immunological parts that collectively maintain intestinal homeostasis. The biochemical barrier includes secreted mucins and antimicrobial peptides, while the physical barrier is made of a single layer of specialized cells such as enterocytes, goblet cells, enteroendocrine cells, Paneth cells, and M cells. Immune cells in the LP, such as macrophages, dendritic cells, T cells, and mast cells, interact with the epithelium to maintain barrier integrity and immune functions. IgA, immunoglobulin A. Adapted from Untersmayr et al., 2022 [11].*

Enterocytes are the most abundant cell type lining the villi and are specialized for nutrient absorption. Enteroendocrine and goblet cells are scattered throughout the epithelium and secrete various hormones or mucus [12]. Goblet cells produce the mucus layer that serves as the first line of physical defense in the gut and prevents microbes from making direct contact with the epithelial layer. Highly glycosylated proteins, such as mucin-2, form this mucus layer, which is critical for disease prevention [13]. Tuft cells are a rare type of chemosensory cell located on the villi and have apical microvilli themselves. They can detect luminal contents, such as allergens, bacteria, and parasitic helminths, and secrete signaling molecules that regulate appropriate immune responses [14]. Paneth cells are located at the bottom of the crypts and secrete antimicrobial peptides (AMPs), including α-defensins and lysozyme, as well as cytokines [11,15,16]. M cells are specialized IECs that lack microvilli. They typically overlay mucosal lymphoid tissue, capture luminal antigens, transport them to Peyer's patches via transcytosis, and modulate secretory immunoglobulin A (IgA) [17,18].

The remainder of the crypt comprises pluripotent stem cells and a proliferative progenitor compartment, which replace old or damaged cells shed at the tips of the villi [12,19]. The large intestine maintains many of the same cells and features of the small intestine but lacks villi, instead containing deep tubular pits that increase in depth as they progress towards the rectum [2,20]. The large intestine features a mucus bilayer, unlike the small intestine's single mucus layer. The loose outer layer contains numerous microbiotas, while the dense inner layer, which adheres closely to the tissue, is mostly free of bacteria. This inner layer has been proposed to function as a physical barrier, separating the luminal microbiota from the epithelial barrier [21–23]. Collectively, these cells coordinate nutrient absorption, establish and maintain both biochemical and physical barriers that prevent the translocation of endotoxins, pathogens, and dietary antigens, and regulate the secretion of immunological mediators [1,6,11].

1.2 Intestinal barrier: its function as a modulator of human health and disease

The intestinal barrier has been extensively studied and is a central focus for understanding the relationship between the body's external environment and disease development. In recent years, the incidence of allergic, autoimmune, and metabolic diseases has reached almost epidemic proportions [24]. It has been suggested that the swift rise in the occurrence of these conditions may be attributed to the disruption of the intestinal epithelial barrier caused by external exposome factors [25]. Environmental exposures, including chemicals, pollutants, tobacco smoke, lifestyle choices, and dietary habits, are increasingly implicated in human health and are identified as contributing factors in the initiation and exacerbation of intestinal epithelial inflammation and increased permeability [26,27].

The intestinal barrier functions as a selectively permeable membrane, exhibiting an inherent permeability that facilitates efficient absorption of nutrients and electrolytes whilst concurrently protecting underlying tissues from luminal microorganisms and antigens [1,6]. This balance is maintained through coordinated epithelial and immune mechanisms that act as physical and chemical barriers. When barrier integrity is compromised, microbial products, pathogens, and toxic digestive metabolites can pass from the gut into the bloodstream, thereby triggering or perpetuating pathological inflammation, activating the immune system, and contributing to disease development [24,28]. This barrier failure, commonly known as leaky gut, has been implicated in the onset or development of inflammatory bowel disease (IBD), metabolic dysfunction–associated steatotic liver disease (MASLD), colorectal cancer, rheumatoid arthritis, and neurodegenerative disorders such as Parkinson's and Alzheimer's disease [5,11,26,28–30].

In leaky gut, the intestinal wall fails to effectively separate luminal contents from the underlying immune system due to compromised tight junctions in IECs [31,32]. These tight junctions, together with adherens junctions and desmosomes, strongly connect neighboring epithelial cells. They form a physical barrier and enable

paracellular transport through the intestinal barrier via a highly selective “pore” pathway or a less selective “leak" pathway [33]. Additionally, they serve as a mechanical boundary between the intestinal lumen and the deeper layers of the intestinal barrier [34]. Tight junctions are highly dynamic, molecularly complex structures. Located at the apical surface of epithelial cells, tight junctions are composed of transmembrane proteins and signaling molecules that link to the cytoskeleton via scaffolding proteins such as zonula occludens, occludin, claudins, and junctional adhesion molecules (JAMs). Together, these components enable the swift adaptation of the intestinal barrier in response to physiological forces and environmental stimuli [1,5,35].

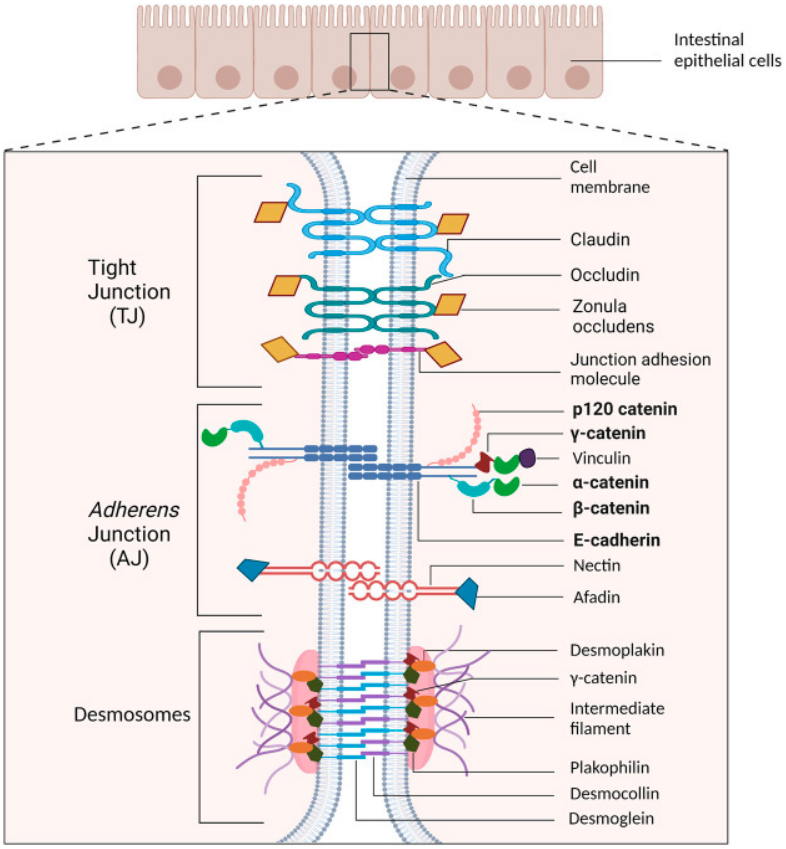

Figure 2: Schematic overview of cell–cell adhesion complexes in intestinal epithelial cells. *IECs are connected by junctions along the apical–basal axis. Tight junctions at the apical region regulate polarity and permeability. Adherens junctions below tight junctions aid cell–cell adhesion, and desmosomes further provide mechanical stability at the base. Adapted from Lessey et al., 2022 [36].*

Beneath the epithelial layer resides the LP, a layer of loose connective tissue and interstitial matrix. This layer functions as a critical interface for the body's innate and adaptive immune responses and plays a role in the chemical barrier of the intestinal epithelium [37]. While the chemical barrier of the intestine is supported by the mucus and epithelial layers, the LP is a major site of intestinal immunity. The LP is colonized by macrophages, dendritic cells, innate lymphoid cells, isolated lymphoid follicles, CD4+ and CD8+ T cells, as well as IgA-secreting plasma cells [38]. Collectively, these cells help maintain the gut mucosal barrier and protect it from pathogen invasion by rapidly stimulating innate and adaptive immune responses through antigen presentation, cytokine secretion, and antibody production [38–40]. Under homeostatic conditions, these immune cells regulate the proliferation, differentiation, and apoptosis of the intestinal epithelium. In contrast, a leaky gut causes abnormal production of pro- and anti-inflammatory mediators, disrupting the tightly regulated immune system and contributing to chronic gut inflammation and progressive damage to the intestinal epithelium [6,41].

1.3 Nitric oxide homeostasis and the development of intestinal barrier dysfunction

It is now widely recognized that the function and maintenance of the intestinal barrier are governed by intricate molecular mechanisms and signaling pathways. One pathway in particular, the inducible nitric oxide synthase (iNOS) pathway, has been identified as a critical contributor to the development of intestinal barrier dysfunction [42]. Nitric oxide synthase (NOS) consists of three isoforms: neuronal NOS (nNOS; NOS1), inducible NOS (iNOS; NOS2), and endothelial NOS (eNOS; NOS3). Via the NOS pathway, L-arginine (L-arg) is enzymatically converted into L-citrulline and nitric oxide (NO), a signaling molecule that plays significant roles in vasodilation and immune responses regulation [43]. This reaction is mediated by calmodulin (CaM) binding between iNOS's oxygenase and reductase domains and involves an elaborate electron transport chain that requires five cofactors: nicotinamide adenine dinucleotide phosphate (NADPH), flavin adenine dinucleotide (FAD), flavin mononucleotide (FMN), heme, and tetrahydrobiopterin (BH_4) [32,44].

NOS enzyme activity is controlled at multiple levels, including substrate and cofactor availability, protein–protein interactions, transcriptional and post-transcriptional mechanisms, and intracellular signaling pathways [45]. In contrast to other NOS isoforms, iNOS is primarily regulated at the transcriptional level [46]. Pro-inflammatory cytokines, including tumor necrosis factor-α (TNF-α), interferon-γ (IFN-γ), and interleukin-1 (IL-1), along with the endotoxin lipopolysaccharide (LPS), are major inducers of iNOS expression [47]. These factors bind to cell-surface receptors and activate intracellular kinases, which phosphorylate downstream proteins and activate transcription factors such as nuclear factor κB (NF-κB) and signal transducer and activator of transcription 1α (STAT-1α). These transcription factors translocate to the nucleus, bind to the iNOS promoter, and induce iNOS gene expression [45,48].

Further regulation of iNOS is mediated by Arginase 2 (Arg2). Arg2 is a mitochondrial enzyme found in inflammatory macrophages and serves as an endogenous inhibitor of iNOS activity by utilizing L-arginine as a substrate [49,50]. Arg2 catalyzes the conversion of L-arginine into L-ornithine and urea. L-ornithine functions as a precursor for polyamines and proline, which are vital for cell proliferation, collagen synthesis, and tissue repair. Meanwhile, urea is required for the disposal of nitrogen [43,51]. Additionally, arginases are thought to limit NO synthesis by uncoupling NOS, thereby generating superoxide and peroxynitrite. They are also suggested to suppress iNOS translation and stability, inhibit iNOS activity via urea production, and increase NOS sensitivity to asymmetric dimethyl-L-arginine, a natural NOS inhibitor [32,51].

In the intestinal epithelium, iNOS uses L-arginine to generate NO, which modulates epithelial permeability by affecting tight-junction organization and cytoskeletal dynamics [52]. NO is soluble in both water and lipids, allowing rapid diffusion across biological membranes without the need for receptors or channels [53,54]. Together, with its short half-life of approximately 3–5 seconds, these properties enable NO to stimulate and activate groups of neighboring cells simultaneously [52].

Under physiological conditions, NO is generated at picomolar concentrations and acts as a protective agent. It is then rapidly scavenged by interactions with

hemoglobin in red blood cells [55,56]. Nitrate and nitrite, oxidative end products of NO metabolism, can serve as iNOS-independent sources of NO [48]. When iNOS is induced, NO is produced at micromolar concentrations, exerting potent antimicrobial and immunoregulatory effects that persist until the enzyme is degraded [45,48,57]. Due to the increased amount of NO produced by iNOS, NO is unable to be completely scavenged by hemoglobin. Consequently, NO can react with superoxide anions, primary oxygen radicals generated at inflammatory sites, leading to the formation of peroxynitrite ($ONOO^-$) or the nitronium ion (NO_2^+) [55,56]. These highly reactive and toxic intermediates can induce protein nitrosylation and tyrosine nitration, and have also been shown to impair intestinal barrier function by disrupting signaling pathways that regulate tight junction proteins [58,59].

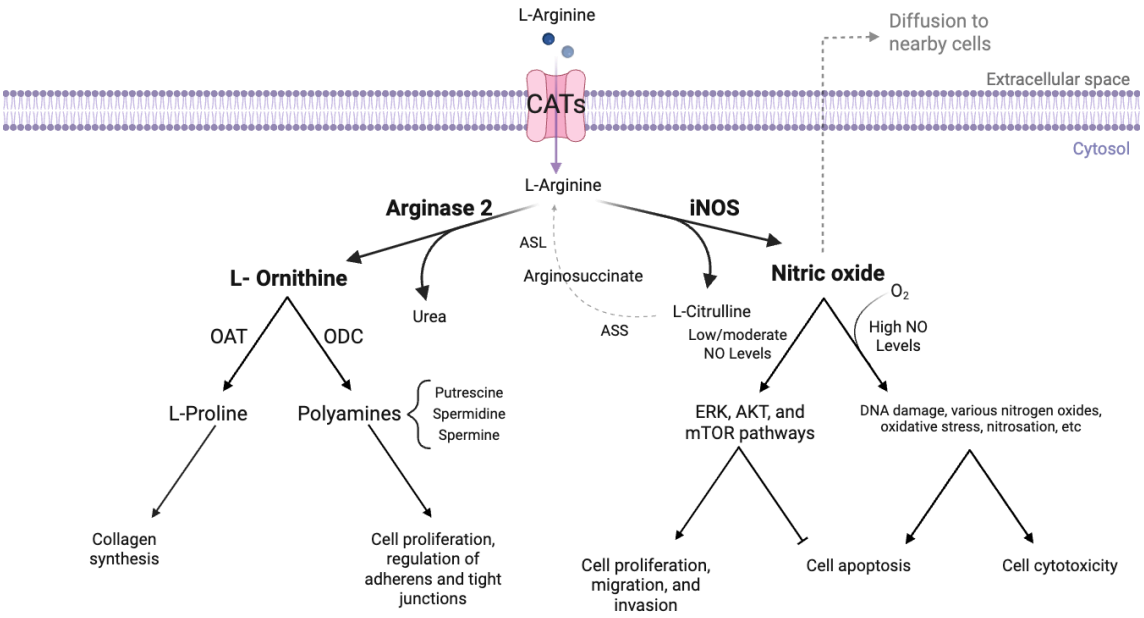

Figure 3: Overview of L-arginine transport, metabolism, and downstream cellular effects. *L-arginine is transported into the cell via cationic amino acid transporters (CATs) and can be metabolized by Arg2 to generate urea and L-ornithine, or by iNOS to produce NO and L-citrulline. L-ornithine serves as a precursor for polyamine synthesis via ornithine decarboxylase (ODC) or for L-proline production via ornithine aminotransferase (OAT), thereby contributing to cell proliferation, regulation of adherens and tight junctions, and collagen synthesis. NO exerts concentration-dependent effects, promoting signaling through the ERK, AKT,*

and mTOR pathways at low to moderate levels, whereas high NO levels induce oxidative and nitrosative stress, DNA damage, apoptosis, and cytotoxicity. Created with BioRender.com and adapted from concepts described in Niu et al., 2022 [60].

Therefore, maintaining strict regulation of iNOS activity is crucial for proper physiological functioning. Overexpression or dysregulation of iNOS, leading to excessive NO levels, can cause toxic effects associated with various diseases, including septic shock, diabetes, cancer, endocrine disorders, insulin resistance, and metabolic syndrome [45,61]. The dynamic interplay among L-arg, iNOS, and Arg2 in the small intestine constitutes an important regulatory axis governing intestinal permeability and disease. Current research shows that intestinal NO homeostasis and arginine metabolism are mediated by arginase and NO synthesis in aging mice and have been implicated in "inflammaging" and barrier dysfunction [42]. Emerging evidence also indicates that the Arg2–iNOS axis in enterocytes is a potential therapeutic target for preserving barrier integrity [43]. And lastly, studies on the loss of Arg2 have linked increased arginine availability to enhanced NO production, suggesting that Arg2 regulates arginine pools and NO synthesis [62]. With that said, the physiological role of Arg2 in NO homeostasis and intestinal barrier regulation remains incompletely understood.

1.4 Hypothesis and Research Questions

The results of previous studies employing animal models of MASLD and aging suggest that dysregulation of arginase activity in small intestinal tissue is related to impaired intestinal barrier function. Based on the assumption that Arginase 2 in enterocytes plays a critical role in nitric oxide homeostasis and, subsequently, intestinal barrier function, this work investigates the following hypothesis:

Enterocyte-specific knockout Arginase-2 mice have altered nitric oxide homeostasis and thereby altered intestinal barrier function.

The hypothesis will be investigated using the following questions:

1) Is the nitric oxide homeostasis altered in the intestine of Arg2 knockout mice?
2) Is the loss of Arg2 in enterocytes related to changes in intestinal barrier function?

2. Materials and Equipment

2.1 General Equipment and Materials

Materials and Equipment	Manufacturer
2.8 mm Zirconium oxide beads	Bio Cat GmbH, Heidelberg, Germany
96-Well Plate	VWR International, LLC, Radnor, USA
Aluminum foil ROTILABO®	Carl Roth GmbH + Co. KG, Karlsruhe, Germany
CLARIOstar® Plus Microplate Reader	BMG Labtech, Ortenberg, Germany
Cold Block	Laboratory Stock, University of Vienna, Vienna, Austria
Dewar transport vessel (liquid nitrogen container)	KGW-Isotherm Karlsruhe Glastechnisches Werk –Schieder GmbH, Karlsruhe, Germany
Eppendorf Research® plus Pipette (2.5 µL,10 µL, 20 µL, 100 µL, 200 µL, 300 µL (multi-channel), 1000 µL, 5000 µL)	Eppendorf SE, Hamburg, Germany
Eppendorf tubes (0,5mL, 1,5mL, 2mL)	SARSTEDT AG & Co. KG, Nümbrecht, Germany
Eppi Stand	Laboratory Stock, University of Vienna, Vienna, Austria
Falcons (15mL, 50mL)	SARSTEDT AG & Co. KG, Nümbrecht, Germany
Foam Ice box	Laboratory Stock, University of Vienna, Vienna, Austria
Freezer Liebherr ProfiLine	Liebherr-International Germany GmbH, Biberach an der Riß, Germany
Fridge Liebherr ProfiLine	Liebherr-International Germany GmbH, Biberach an der Riß, Germany
HERMLE Z 216 MK centrifuge	Hermle Labortechnik GmbH, Wehingen, Germany
Ice machine FM-120KE-50-HC	Hoshizaki Europe B.V. – HQ, Amsterdam, Netherlands
Kimtech™ precision wipes	Kimberly-Clark Worldwide, Inc., Koblenz/Rheinhafen, Germany
Micro tube 2mL	SARSTEDT AG & Co. KG, Nümbrecht, Germany
Mixing Block MB-102	BIOER Technology, Zhejiang, China
ONILAB Minicentrifuge – D1008	ONILAB, Ningbo, Zhejiang, China
Orion pH-Meter Five Easy	Mettler-Toledo GmbH, Columbus, USA

PCE MSP-100 Magnetic Stirrer	PCE-Instruments, Meschede, Germany
Peleus ball	DLAB SCIENTIFIC CO., LTD, Peking, China
Permanent marker, alcohol-resistant	SARSTEDT AG & Co. KG, Nümbrecht, Germany
PHOENIX Instrument Vortexer RS-VA10	Phoenix Instrument GmbH, Garbsen, Germany
Pipette tips (10 µL, 100 µL, 200 µL, 1000 µL, 5000 µL)	SARSTEDT AG & Co. KG, Nümbrecht, Germany
Precellys® 24 Touch Homogenizer	Bertin Technologies, Montigny-le-Bretonneux, France
Razor Blades	Laboratory Stock, University of Vienna, Vienna, Austria
Ruler	Laboratory Stock, University of Vienna, Vienna, Austria
Scissors	Laboratory Stock, University of Vienna, Vienna, Austria
Serological pipette (5mL, 10mL, 25mL)	SARSTEDT AG & Co. KG, Nümbrecht, Germany
StarGuard® nitrile gloves	Starlab GmbH, Hamburg, Germany
Tape	Laboratory Stock, University of Vienna, Vienna, Austria
VWR® LA Classic, Analytical Balances	VWR International, LLC, Radnor, USA
Water BioScience Grade, sterile, nuclease-free, autoclaved	Carl Roth GmbH + Co. KG, Karlsruhe, Germany
Weighing trays	Laboratory Stock, University of Vienna, Vienna, Austria

Chemicals	**Manufacturer**
2-Propanol ≥ 99,5% (C_3H_8O)	Carl Roth GmbH + Co. KG, Karlsruhe, Germany
Bovines Serum albumin (BSA) fraction V ≥ 98%	Carl Roth GmbH + Co. KG, Karlsruhe, Germany
Distilled Water (dH_2O)	Laboratory Stock, University of Vienna, Vienna, Austria
Double Distilled Water (ddH_2O)	Laboratory Stock, University of Vienna, Vienna, Austria
Ethanol 70%	Laboratory Stock, University of Vienna, Vienna, Austria
Ethanol, absolute for analysis, EMSURE®	Sigma-Aldrich, St. Louis, USA
Hydrochloric Acid 37% (HCl)	Carl Roth GmbH + Co. KG, Karlsruhe, Germany
Liquid nitrogen	University of Vienna, Vienna, Austria

Methanol ≥99.8%, ACS reagent (CH_4O)	Sigma-Aldrich, St. Louis, USA
Potassium Chloride (KCl)	Carl Roth GmbH + Co. KG, Karlsruhe, Germany
Sodium Chloride (NaCl)	Carl Roth GmbH + Co. KG, Karlsruhe, Germany
Sodium Hydroxide 6 N (NaOH)	Carl Roth GmbH + Co. KG, Karlsruhe, Germany
Urea ≥ 99,5%, p.a., ultra quality (CH_4N_2O)	Carl Roth GmbH + Co. KG, Karlsruhe, Germany

2.2 Everted Gut Sac Model

Materials and Equipment	**Manufacturer**
Duodenum from Arg2 KO Mice	Breeding by the SPF Animal Facility of the University of Vienna, Vienna, Austria
Gavage Needle	Laboratory Stock, University of Vienna, Vienna, Austria
Glass Petri Dishes	Laboratory Stock, University of Vienna, Vienna, Austria
Glass Pipettes	Carl Roth GmbH + Co. KG, Karlsruhe, Germany
MAXIMA® (1 mL) disposable syringe	Henry Schein Services GmbH, Langen, Germany
Mixing Block MB-102	BIOER Technology, Zhejiang, China
Sewing thread, extra strong M 782, 100% polyester	Gütermann GmbH, Gutach-Breisgau, Germany
Sterican® Single Use Hypodermic Needle	B. Braun Austria GmbH, Maria Enzersdorf, Austria
Tissue Scissors	Laboratory Stock, University of Vienna, Vienna, Austria
Tweezers	Laboratory Stock, University of Vienna, Vienna, Austria
Water Bath	GFL Gesellschaft für Labortechnik GmbH, Burgwedel, Germany

Chemicals	**Manufacturer**
Acetic acid 100% ($C_2H_4O_2$)	Carl Roth GmbH + Co. KG, Karlsruhe, Germany
Benzoic acid ($C_7H_6O_2$)	Carl Roth GmbH + Co. KG, Karlsruhe, Germany
Calcium chloride dihydrate ≥ 99% ($CaCl_2$ x 2 H_2O)	Carl Roth GmbH + Co. KG, Karlsruhe, Germany
D (+)-Xylose ($C_5H_{10}O_5$)	Merck KGaA, Darmstadt, Germany

Dulbecco's Phosphate Buffered Saline (DPBS)	Sigma-Aldrich Chemie GmbH, Taufkirchen, Germany
Gas Mixture (95% O_2, 5% CO_2)	Air Liquide Austria GmbH, Schwechat, Austria
HEPES (PUFFERAN®) ≥ 99,5% ($C_8H_{18}N_2O_4S$)	Carl Roth GmbH + Co. KG, Karlsruhe, Germany
Magnesium sulfate, anhydrous ≥ 99,5% ($MgSO_4$)	ThermoFisher GmbH, Kandel, Germany
Potassium chloride ≥ 99,5% (KCl)	Carl Roth GmbH + Co. KG, Karlsruhe, Germany
Potassium dihydrogen phosphate ≥ 99% (KH_2PO_4)	Carl Roth GmbH + Co. KG, Karlsruhe, Germany
Sodium chloride (NaCl)	Carl Roth GmbH + Co. KG, Karlsruhe, Germany

2.3 Xylose Permeability Assay

Materials and Equipment	**Manufacturer**
Floating Eppi Foam Holder	Laboratory Stock, University of Vienna, Vienna, Austria

Chemicals	**Manufacturer**
Hydrochloric Acid 37% (HCl)	Carl Roth GmbH + Co. KG, Karlsruhe, Germany
Acetic Acid 100% ($C_2H_4O_2$)	Carl Roth GmbH + Co. KG, Karlsruhe, Germany
Phloroglucinol Dihydrate ≥ 98% ($C_6H_6O_3$ x $2H_2O$)	Carl Roth GmbH + Co. KG, Karlsruhe, Germany

2.4 Griess Assay

Materials and Equipment	**Manufacturer**
Griess Reagent System	Promega Corporation, Madison, USA

Chemicals	**Manufacturer**
Dulbecco's Modified Eagle Medium (DMEM)	PAN-Biotech GmbH, Aidenbach, Germany

2.5 Arginase Activity Assay

Chemicals	**Manufacturer**
Alpha-Isonitrosopropiophenone (Alpha – ISPF)	Sigma-Aldrich, St. Louis, USA
L-Arginine	Sigma-Aldrich, St. Louis, USA
Manganese (II) Chloride Tetrahydrate $MnCl_2$*$4H_2O$	Thermo Fisher (Kandel) GmbH, Kandel, Germany

Ortho-phosphoaisc acid 85% (H_3PO_4)	Carl Roth GmbH + Co. KG, Karlsruhe, Germany
Protease Inhibitor cocktail	Sigma-Aldrich, St. Louis, USA
Sulphuric Acid (1N) H_2SO_4	Carl Roth GmbH + Co. KG, Karlsruhe, Germany
Tris-Hydrochlorid PUFFERRAN® ≥ 99,9%	Carl Roth GmbH + Co. KG, Karlsruhe, Germany
Triton® X 100	Carl Roth GmbH + Co. KG, Karlsruhe, Germany

2.6 RNA Isolation

Chemicals	**Manufacturer**
Chloroform: Isoamyl Alcohol 24:1 ($CHCl_3$)	PanReac AppliChem, Castellar del Vallès, Spain
TRItidy G™ (Trizol)	AppliChem GmbH, Darmstadt, Germany
Water BioScience Grade, sterile, nuclease-free, autoclaved	Carl Roth GmbH + Co. KG, Karlsruhe, Germany

2.7 Protein Extraction

Materials and Equipment	**Manufacturer**
Micro-Homogenizer (Pellet Plunger)	Carl Roth GmbH + Co. KG, Karlsruhe, Germany

Chemicals	**Manufacturer**
DL-Dithiothreitol ≥ 99% ($CH(OH)CH_2SH)_2$ (DTT)	Sigma-Aldrich, St. Louis, USA
Guanidine hydrochloride ≥ 99,5% (CH_5N_3 – HCl)	Carl Roth GmbH + Co. KG, Karlsruhe, Germany
Micro-Homogenizer (Pellet Plunger)	Carl Roth GmbH + Co. KG, Karlsruhe, Germany
Phosphatase Inhibitor Cocktail 2	Sigma-Aldrich, St. Louis, USA
Phosphatase Inhibitor Cocktail 3	Sigma-Aldrich, St. Louis, USA
Protease inhibitor cocktail	Sigma-Aldrich, St. Louis, USA
Water, ROTIPURAN®	Carl Roth GmbH + Co. KG, Karlsruhe, Germany

2.8 Bradford Protein Determination Assay

Materials and Equipment	**Manufacturer**
Color reagent tray	Laboratory Stock, University of Vienna, Vienna, Austria

Chemicals	**Manufacturer**

Bio-Rad Protein Assay Dye Reagent Concentrate	Bio-Rad Laboratories Inc., Hercules, USA

2.9 Western Blot

Materials and Equipment	**Manufacturer**
Blotting Tweezers	Laboratory Stock, University of Vienna, Vienna, Austria
ChemiDocTM MP Imaging Systems	BioRad Laboratories, Hercules, USA
Extra Thick Western Blotting Filter Paper (20 cm x 20 cm)	Thermo Fisher Scientific, Massachusetts, USA
Immuno-Blot® PVDF Membranes	BioRad Laboratories, Hercules, USA
Impulse hand sealer	Rotek Handels GmbH, Hagenbrunn, Austria
Mini-PROTEAN® Tetra Handcast Systems	BioRad Laboratories, Hercules, USA
ONILAB LED Digital Orbital Shakers – SK-O180-S	ONILAB, Ningbo, Zhejiang, China
PowerPac™ HC High-Current Power Supply	BioRad Laboratories, Hercules, USA
PS-M3D Variable Speed / Angle, Multi-Function 3D Rotator	Grant Instruments, Shepreth, Cambridgeshire, UK
Rotilabo Rundfilter, Typ 601A	Carl Roth GmbH&Co.KG, Karlsruhe, Germany
Trans-Blot® TurboTM Transfer System	BioRad Laboratories, Hercules, USA

Chemicals	**Manufacturer**
β- Actin Antibody (C4), mouse monoclonal IgG	Santa Cruz Biotechnology, Dallas, USA
2-Mercaptoethanol ≥99%, p.a. (C2H6OS)	Carl Roth GmbH + Co. KG, Karlsruhe, Germany
Acetic acid 100% ($C_2H_4O_2$)	Carl Roth GmbH + Co. KG, Karlsruhe, Germany
Acrylamide/Bis-solution 30, ROTIPHORESE® 30%	Carl Roth GmbH + Co. KG, Karlsruhe, Germany
Ammonium peroxydisulphate ≥98%, extra pure ($(NH_4)_2S_2O_8$)	Carl Roth GmbH + Co. KG, Karlsruhe, Germany
Anti-rabbit IgG, HRP-linked Antibody	Cell Signaling Technology, Danvers, USA
Arginase -2 (D9J1N) XP® Rabbit mAb	Cell Signaling Technology, Danvers, USA
Bromophenol Blue ($C_{19}H_{10}Br_4O_5S$)	Carl Roth GmbH + Co. KG, Karlsruhe, Germany
Clarity™ Western ECL Substrate	BioRad Laboratories, Hercules, USA

Glycerol ≥99.5% ($C_3H_8O_3$)	Sigma-Aldrich, St. Louis, USA
Glycine ($C_2H_5NO_2$)	Carl Roth GmbH + Co. KG, Karlsruhe, Germany
N,N,N',N'-Tetramethylethylenediamine (TEMED) ≥99% ($C_6H_{16}N_2$)	Carl Roth GmbH + Co. KG, Karlsruhe, Germany
Nonfat dried milk powder	ITW Reagents, Darmstadt, Germany
Occludin Antibody (OC-3F10)	Thermo Fisher Scientific, Massachusetts, USA
Ponceau S ($C_{22}H_{12}N_4Na_4O_{13}S_4$)	Carl Roth GmbH + Co. KG, Karlsruhe, Germany
Precision Plus ProteinTM Dual Color Standards	BioRad Laboratories, Hercules, USA
proAnti-mouse IgG, HRP-linked Antibody	Cell Signaling Technology, Danvers, USA
Sodium Chloride CELLPURE® ≥ 99,5% (NaCl)	Carl Roth GmbH + Co. KG, Karlsruhe, Germany
Sodium dodecyl sulphate (SDS) ($C_{12}H_{25}NaO_4S$)	Sigma-Aldrich, St. Louis, USA
Tris-(hydroxymethyl)-aminomethan (Tris) PUFFERRAN® ≥ 99,9% ($C_4H_{11}NO_3$)	Carl Roth GmbH + Co. KG, Karlsruhe, Germany
Tween® 20 ($C_{58}H_{114}O_{26}$)	Carl Roth GmbH + Co. KG, Karlsruhe, Germany

2.10 Tissue Paraffin Embedding and Sectioning

Materials and Equipment	**Manufacturer**
Embedding Station: Cry Console, Dispensing Console, Thermal Console AP250	Microtom International GmbH, Walldorf, Germany
Embedding Trays	Weckert Labortechnik, Kitzingen, Germany
Filter Paper	Carl Roth GmbH + Co. KG, Karlsruhe, Germany
Incubator	Memmert GmbH + Co. KG, Schwabach, Germany
Low Profile Microtome Blades	Leica Biosystems Nussloch GmbH, Nussloch, Germany
Microtome Leica RM2245	Leica Microsystems CMS GmbH, Wetzlar, Germany
Paraffin stretch bath GFL 1052	LAUDA DR. R. WOBSER GMBH & CO. KG, Lauda-Königshofen, Germany
Superfrost® plus Microscope Slides	Labxperts GmbH, Klosterneuburg, Austria

Tissue Cassettes	Sanova Pharma GesmbH, Wien, Austria

Chemicals	**Manufacturer**
Disodium hydrogen phosphate ≥ 99%, anhydrous (Na_2HPO_4)	Carl Roth GmbH + Co. KG, Karlsruhe, Germany
Ethanol ≥ 99.8%, denatured (C_2H_6O)	Carl Roth GmbH + Co. KG, Karlsruhe, Germany
Ethanol 96% (C_2H_6O)	Carl Roth GmbH + Co. KG, Karlsruhe, Germany
Formaldehyde solution, acid-free 37%	Carl Roth GmbH + Co. KG, Karlsruhe, Germany
Phosphate Buffered Saline (PBS)	Laboratory Stock, University of Vienna, Vienna, Austria

2.11 Tissue Staining

Materials and Equipment	**Manufacturer**
A-PAP Pen	Daido Sangyo Co Ltd, Japan
Aponorm Hydrogen Peroxide Solution 3%	Auge Gottes Apotheke, Vienna, Austria
CO2 Incubator MCO-170AIC	Panasonic, Osaka, Japan
Dako Liquid DAB+ Substrate Chromogen System	Agilent Technologies, Inc., Santa Clara, USA
Entellan™ Mounting Media	Sigma Aldrich (Merck KGaA), Darmstadt, Germany
Epredia™ SuperFrost Plus™ Adhesion slides	Thermo Fisher Scientific, Massachusetts, USA
Glass Dying Vat	Sanova Pharma GesmbH, Wien, Austria
Glass Insert for Dying Vat	Sanova Pharma GesmbH, Wien, Austria
Glass Rod	Carl Roth GmbH + Co. KG, Karlsruhe, Germany
StainTray™	Simport Scientific Inc., Saint-Mathieu-de-Beloeil, Kanada
VWR® Rectangular Cover Glasses 24x50 mm	VWR International, LLC, Radnor, USA

Chemicals	**Manufacturer**
Alcoholic Eosin Y Solution	Sigma-Aldrich, St. Louis, USA
Goat pAB to Rabbit IgG (HRP Polymer) Solution	Abcam, Cambridge, UK
Aponorm Hydrogen Peroxide Solution 3%	Auge Gottes Apotheke, Vienna, Austria

Arginase -2 (D9J1N) XP® Rabbit mAb	Cell Signaling Technology, Danvers, USA
Arginase-1 (D4E3M™) XP® Rabbit mAb	Cell Signaling Technology, Danvers, USA
Dako Liquid DAB+ Substrate Chromogen System	Agilent Technologies, Inc., Santa Clara, USA
Ethanol ≥ 99,8%, denatured (C_2H_6O)	Carl Roth GmbH + Co. KG, Karlsruhe, Germany
Ethanol 70% (C_2H_6O)	Laboratory Stock, University of Vienna, Vienna , Austria
Ethanol 95% (C_2H_6O)	Carl Roth GmbH + Co. KG, Karlsruhe, Germany
Hematoxylin Solution	Carl Roth GmbH + Co. KG, Karlsruhe, Germany
Immersol® Immersion Oil 518 N	Carl Zeiss Microscopy Germany GmbH, Oberkochen, Germany
Occludin Antibody	Thermo Fisher Scientific, Massachusetts, USA
Protease from *Streptomyces griseus*	Sigma-Aldrich, St. Louis, USA
Roti-Histol	Carl Roth GmbH + Co. KG, Karlsruhe, Germany
Tap Water	Laboratory Stock, University of Vienna, Vienna, Austria

2.12 Triglyceride Quantification

Materials and Equipment	**Manufacturer**
BANDELIN SONOPULS HD 2070 Homogenizer	BANDELIN electronic GmbH & Co. KG, Berlin, Germany
Concentrator plus, Vaccum Concentrator	Eppendorf SE, Hamburg, Germany
MiniBatch D9 Homogenizer and Dispenser	MICCRA GmbH, Buggingen, Germany
Triglycerides (TRIGS) Kit	Randox Teoranta, Donegal, Ireland
Ultrasonic Sonorex Digitec DT	BANDELIN electronic GmbH & Co. KG, Berlin, Germany

2.13 Software

Software	**Manufacturer**
Bio-Rad CRF Manager 3.1	Bio-Rad Laboratories Inc., Hercules, USA
BioRender®	BioRender, Toronto, Kanada
GraphPad Prism 7.0	GraphPad Software Inc., La Jolla, USA
Image Lab 6.1 Software	Bio-Rad Laboratories Inc., Hercules, USA

Leica application suite 4.5	Leica Microsystems GmbH, Wetzlar, Germany
Leica application suite X (LAS X)	Leica Microsystems GmbH, Wetzlar, Germany
MARS Data Analysis Software	BMG Labtech, Ortenberg, Germany
Microplate Manager®	Bio-Rad Laboratories Inc., Hercules, USA
Microsoft Office 365	Microsoft Corporation, Redmond, USA

3. Methods

3.1 Arg-2 Mice: Handling and Sample Collection

All procedures in animals were performed in a specific pathogen-free barrier (SPF) facility accredited by the Association for Assessment and Accreditation of Laboratory Animal Care (AAALAC). All animals were bred and maintained under SPF conditions at the University of Vienna animal facility. Environmental conditions were controlled (12 h/12 h light/dark cycles, ~23 °C, ~55% relative humidity), and mice had ad libitum access to tap water. Enterocyte-specific Arg2 knockout (KO) mice were generated by crossing Arg2 lox/lox mice (a generous gift from Prof. Firsov, Department of Pharmacology and Toxicology, University of Lausanne, Switzerland) [63] with B6.Cg-Tg (Vil1-cre) 1000Gum/J mice (The Jackson Laboratory, Bar Harbor, USA). Littermates lacking enterocyte-specific Arg2 deletion but sharing the same genetic background as KO mice were designated as Arg2 wild-type (WT). For the following investigation, male young mice (3-5 months old) were used. In the first sampling, tissue samples were collected from n=9 naïve Arg2 KO and WT mice after cervical dislocation. In the second sampling, tissue samples were obtained from n=8 animals as part of an animal experiment approved by the local Institutional Animal Care and Use Committee (BMBWF, 2022-0.527.442). Animals were anesthetized with a mixture of ketamine/xylazine (100 mg ketamine/kg body weight and 16 mg xylazine/kg body weight, i.p. injection) and euthanized by cervical dislocation. Portions of the small intestine were removed and used for the ex vivo everted gut-sac method, while other tissue portions were snap-frozen in liquid nitrogen or fixed in 4% phosphate-buffered saline (PBS)-buffered formaldehyde solution for further analysis.

3.2 Everted Gut Sac Model to Assess Intestinal Permeability

An ex vivo everted gut-sac model was used to assess intestinal permeability in Arg2 WT and Arg2 KO mice. The experimental procedures were performed by members of the working group. In this model, the transport of substances from the mucosal to the serosal side of the small intestine serves as a measure of intestinal permeability

[64]. The method was adapted from Hamilton and Butt [65], and is described briefly below.

Small-intestinal tissue was collected, stored in ice-cold DPBS, and then transferred to Krebs–Henseleit–bicarbonate buffer supplemented with 0.2% bovine serum albumin (KRH buffer) (Table 14, Supplementary Information). The intestine was cut into equal-length segments, everted over a gavage needle, and tied at one end with sewing thread. Each segment was filled with KRH buffer and tied at the opposite end to form a sealed sac. Sac length, weight, and filling volume were recorded.
Tissue sacs were incubated for 5 min at 37 °C in gassed (95% O_2/5% CO_2) KRH buffer with 0.1% xylose (Table 14, Supplementary Information). Incubation was stopped by transferring the sacs to ice-cold KRH buffer, after which the serosal contents were collected for subsequent xylose permeability analysis.

3.3 Xylose Permeability Assay to Assess Intestinal Barrier Function

The xylose permeability assay is widely used as an indicator of intestinal function [66]. Samples are heated with an acid mixture, converting xylose to furfural, which then reacts with phloroglucinol to form phloroglucide, producing a red/pink color change measured photometrically at 540 nm [67]. In the present work, liquid samples collected from the everted gut sac method were used, and the assay was performed as described by Hayashi et al. [68].

Table 1: Standard series for xylose permeability measurement

Standard	D(+)- Xylose (mg)	*Solvent (L)	Concentration (mg/L)
Standard 1	52.6	0.5	0.7
Standard 2	97.6	0.5	1.3
Standard 3	195.2	0.5	2.6

*Solvent: 3.9 g Benzoic acid in 1.5 L distilled water

Table 2: Color reagent composition for xylose permeability measurement

Chemicals	Amounts

Acetic Acid 100%	100 mL
Hydrochloric Acid 37%	10 mL
Phloroglucinol dihydrate	0.5 g

Standard solutions and color reagents were prepared as described in Tables 1 and 2 prior to detection. Samples were thawed on ice, vortexed, and centrifuged (1000 rcf, 2 min) to remove insoluble particles. Samples were prepared in triplicate, while standards and blanks were prepared in duplicate. For the assay, 500 µL of color reagent was added to Eppis, followed by 5 µL of sample, standard, or blank (ddH_2O or KRH Buffer, respectively). Samples were heated for 4 mins at 100°C on a mixing block, and the reaction was stopped by cooling the samples to RT in a water bath. Subsequently, 200 µL of samples and standards were pipetted onto a 96-well plate, and absorbance was measured at 540 nm. A linear equation was generated using xylose standards, and xylose concentration (mmol/L) was calculated.

3.4 Nitric Oxide Quantification Using the Griess Assay

A commercially available Griess assay was used to measure nitrite (NO_2^-), a primary, stable, and nonvolatile breakdown product of NO. Based on a reaction with sulfanilamide and N-1-naphthylethylenediamine dihydrochloride (NED), a purple color change is produced, which can then be measured photometrically at 540nm [69]. The assay was performed according to the manufacturer's instructions.

In short, frozen small intestinal tissue was homogenized in 130 µL ice-cold DMEM and centrifuged (13,000 rcf, 20 min, 4°C) after which the supernatant was taken and used for the assay. Protein determination was performed with a dilution factor of 1:30, as described in Section 3.8. For the Griess assay, the standard series was prepared directly in a 96-well plate, as shown in Table 3, in triplicate.

Table 3: Standard series for nitrite determination

Standard	Nitrite Standard (µL)*	Buffer (µL)**	Concentration (µM)

A	80 µL Nitrite Standard	-	100
B	40 µL A	40	50
C	40 µL B	40	25
D	40 µL C	40	12.5
E	40 µL D	40	6.25
F	40 µL E	40	3.13
G	40 µL F	40	1.56
H	-	40	0

*Nitrite Standard from Griess Kit (1:1000) in DMEM. ** Buffer: DMEM

Sulfanilamide and NED solutions were equilibrated to RT, and 40 µL of each sample was pipetted into a 96-well plate in duplicate. Subsequently, 40 µL of Sulfanilamide was added to each well and incubated in the dark for 5-10 mins at RT. After, 40 µL of NED solution was added and incubated again for 5-10 mins at RT in the dark. Absorbance was measured at 540 nm within 30 mins and nitrite concentration (µM) was calculated.

3.5 Assessment of Arginase Activity in Small Intestinal Tissue

Arginase activity was measured in tissue homogenates by quantifying urea generated from the reaction of L-arg in the presence of α-ISPF. In this reaction, a pink color change develops and can be measured photometrically at 540 nm. The assay was performed using a modified version of the protocol by Corraliza et al. [70].

Required solutions for arginase activity are listed in Table 15 (Supplementary Information). Frozen small-intestinal tissue was homogenized in 100 µL of lysis buffer and then centrifuged (13,000 rcf, 10 min, 4 °C). The supernatant was transferred to a new Eppi and used for the remainder of the assay. Samples were diluted 1:10 in lysis buffer and heated for 10 min at 55 °C on a mixing block. All samples were prepared in duplicate with corresponding blanks. Reactions contained 50 µL of the diluted sample and 50 µL of 0.5 M L-arginine or ddH_2O for blanks. Samples were vortexed and incubated for 60 min at 37 °C on a heating block.

Meanwhile, a urea standard series was prepared as a stock solution (Table 4), and 100 µL of each standard was added to two Eppis to be measured in duplicate.

Table 4: Standard series for the measurement of arginase activity

Standard	Solution (µL)	ddH_2O (µL)	Concentration (µg/µL)
A	100 µL *	900	0.8
B	500 µL A	500	0.4
C	500 µL B	500	0.2
D	500 µL C	500	0.1
E	500 µL D	500	0.05
F	500 µL E	500	0.0025
G	500 µL F	1000	0

*Urea Stock Solution: 80 mg Urea in 10 mL ddH_2O (800 µg / 100 µL)

Shortly before the end of the 60-min incubation, 800 µL of the acid mixture was added to each standard and sample Eppi, followed by 50 µL of 9% α-ISPF. All Eppis were then heated for 45 min at 100 °C on a mixing block. Meanwhile, the remaining homogenate was used to determine protein level as described in Section 3.8. After heating, 200 µL of each sample, standard, and blank was pipetted into a 96-well plate, and absorbance was measured photometrically at 540 nm.

3.6 RNA Isolation from Tissue Samples

Total RNA Isolation Reagent (TRIzol) is a monophasic solution of phenol and guanidine isothiocyanate that facilitates the separation of RNA, DNA, and proteins into three phases after adding chloroform and centrifugation [71]. Protein partitions into the organic phase, DNA at the interface, and RNA remains in the aqueous phase. RNA is then precipitated with isopropanol and redissolved in nuclease-free water for further analysis [72]. A commercially available Trizol assay was performed according to the manufacturer's instructions.

In brief, frozen small-intestinal tissue was homogenized in 1 mL of peqGold TriFast (TRIzol) and incubated for 5 min at RT. In the fume hood, 200 µL of chloroform was

added. Samples were hand-shaken vigorously for 20 sec, vortexed for 10 sec, and incubated for 10 min at RT. Samples were centrifuged (12,000 rcf, 10 min, 4°C), and all subsequent steps were performed on ice. The upper aqueous phase was transferred to a new 1.5 mL Eppi, while the lower organic phase was saved for protein extraction. To the aqueous phase, 500 µL of isopropanol was added, followed by vortexing, incubation on ice for 15 min, and centrifugation (12,000 rcf, 10 min, 4°C). The supernatant was discarded, and the pellet was washed twice with 1 mL of 75% ethanol and centrifuged (7,500 rcf, 8 min, 4°C). After air-drying for no more than 10 min, pellets were resuspended in 25 µL of DNase/RNase-free water. RNA samples were heated at 55°C for 10 min on a mixing block and stored at −80°C until further use.

3.7 Protein Extraction using TRIzol

The organic phase obtained from RNA isolation using Trizol can be further used for protein extraction with urea and DTT. The combination of urea and DTT denatures and unfolds complex protein structures, enabling proper protein preparation for downstream applications such as SDS-PAGE [73].

Following the manufacturer's instructions, the organic phase obtained from RNA extraction was thawed and vortexed, then 300 µL of absolute ethanol was added per 1 mL of TRIzol. Samples were vortexed and incubated for 3 min at RT. The supernatant was transferred to a new Eppi and used for the following steps. Approximately 1.5 mL of isopropanol was added. Samples were vortexed, incubated for 10 min at RT, and centrifuged (12,000 rcf, 10 min, 4 °C). The supernatant was discarded, and the pellets were washed three times. For washing, 2 mL of 0.3M guanidinhydrochloride solution was added, incubated for 20 min, centrifuged (7,500 rcf, 5 min, 4 °C), and the supernatant was discarded. Afterward, 2 mL of absolute ethanol was added. Samples were vortexed, incubated for 20 min, ethanol discarded, and the pellets left to air dry. Pellets were resuspended in 10 M urea/50 mM DTT buffer supplemented with protease/phosphatase inhibitor (1 µL/mL), solubilized with a plunger, and incubated for 1 hr at RT. Samples were heated for 5 mins at 100 °C on a mixing block, vortexed, and centrifuged (10,000 rcf, 10 mins, RT).

The supernatant was transferred into a new 0.5 mL Eppi and stored as protein at -80 °C until further use.

3.8 Protein Quantification via Bradford Protein Determination Assay

Protein levels were determined using a method based on Bradford et al., which relies on the binding of Coomassie Brilliant Blue G-250 dye to proteins [74,75]. Upon protein binding, the dye is converted into a stable, unprotonated blue form that can be detected photometrically at 595 nm [75]. Total protein concentration was measured using a commercially available Bradford Protein Assay (Bio-Rad) following the manufacturer's instructions.

Briefly, samples and extraction buffer were diluted 1:30. The Bio-Rad dye reagent was freshly prepared, diluted 1:5 in ddH_2O, and stored in the dark before use. The standard series was prepared as shown in Table 5 using either ddH_2O or extraction buffer. In a 96-well plate, 5 µL of samples or standards was added in triplicate, followed by 200 µL of color reagent per well. After 5 min of shaking, the absorbance was measured at 595 nm. Protein concentrations were calculated using a bovine serum albumin (BSA) standard curve and used to normalize input for subsequent assays.

Table 5: Standard series for protein concentration determination via Bradford assay

Standard	Protein (µL)	Distilled water (µL)	Concentration (mg BSA/mL)
A	2 µL Stock Solution*	198	1.0
B	100 µL A	100	0.5
C	100 µL B	100	0.25
D	100 µL C	100	0.125
E	100 µL D	100	0.0625
F	-	100	0

*Stock Solution: 100 mg BSA/mL distilled water

3.9 Detection of Target Proteins by Western Blot

Western blotting is a technique used to identify specific proteins and typically involves three key steps: protein separation by size, transfer to a solid support, and detection with primary and secondary antibodies [76]. Western blotting was used to assess protein levels of Arginase 2, Occludin, and β-actin.

SDS-PAGE Gel Preparation

SDS-PAGE gels were prepared using Bio-Rad's gel casting system. Spacer and short plates, cleaned with 70% ethanol, were assembled and placed in the gel casting stand. Stock chemicals used for gel preparation are listed in Table 17 (Supplementary Information). A 10% running gel (Table 6) was prepared, poured into the mold, sprayed with 70% ethanol, and polymerized for at least 30 mins. Afterward, ethanol was removed using filter paper, and a 5% stacking gel (Table 6) was prepared and poured on top of the running gel. A 15-well, 1 mm comb was inserted, and the stacking gel polymerized for at least 30 mins. Gels were prepared fresh or used within 72 hrs.

Table 6: Running and stacking gel composition

Chemicals	Running Gel 10% (µL)	Stacking Gel 5% (µL)
dH_2O	4179	1512.5
1.5 M Tris (pH 8.8)	2600	-
0.5 M Tris (pH 6.8)	-	625
30% Acrylamide	3300	312.5
10% SDS	100	25
10% APS	100	25
TEMED	6	3

*Amounts for 2 gels with 1 mm spacer comb.

Sample Preparation and Running SDS-PAGE

Protein concentrations were measured as described in Section 3.8 prior to SDS-PAGE sample preparation. Protein lysates were mixed with buffer (urea/DTT with protease and phosphatase inhibitors) and 4× SDS loading buffer (Table 17,

Supplementary Information). All components except 100 mM DTT were mixed first. The Eppis were vortexed and centrifuged before DTT was added. Samples were then heated for 5 min at 95 °C on a mixing block, vortexed, and centrifuged prior to loading onto the gel. Gels were then inserted into the electrophoresis chamber, filled with 1x electrophoresis buffer (Table 17, Supplementary Information). The spacer comb was removed, and wells were gently washed with 1x electrophoresis buffer. The gels were loaded with 1.5 µL of protein ladder and 10 µL of sample in a predetermined order. Gels were then run at 110 V for 1.5 hrs.

Semi-Dry Protein Transfer

After electrophoresis, gels were gently removed from between the glass plates; the stacking gel and excess running gel were trimmed away, and the gel was placed in Towbin transfer buffer on a shaker for 10 min. Membranes were activated by submersion in methanol for 20 sec, followed by 5 sec in water and 10 min in Towbin buffer. A transfer stack was then prepared: first, filter paper soaked in Towbin buffer was placed in the transfer tray; the activated membrane was placed on top of the filter paper, and the gel, properly oriented, was placed on top of the membrane. The transfer stack was completed with another piece of Towbin-soaked filter paper placed on top of the gel. Towbin buffer was poured over the stack, and the stack was gently rolled once in each direction to remove any air bubbles. The transfer chamber lid was placed on, and the prepared transfer cassette was inserted into the Trans-Blot Turbo system. A standard transfer protocol of 25 V, 1 A, for 30 min was performed, and the membrane was left to dry for at least 1 hr.

Ponceau S Membrane Staining

After drying, the membrane was activated by submersion in 100% methanol for 20 sec, followed by a 5-sec rinse in dH_2O. It was then incubated in Ponceau S stain for 3 min and rinsed again in dH_2O three times for 20 sec each. Ponceau staining was further developed and imaged colorimetrically in the ChemiDoc Imaging System.

Primary and Secondary Antibody Incubation and Detection

After Ponceau S staining and detection, the membrane was rinsed three times for 20 sec each with dH_2O, then blocked for 1 hr in 2.5% BSA in 1× TBST for β-actin and

arginase 2, or in 5% non-fat dried milk in 1× TBST for occludin. After blocking, the membranes were incubated overnight by heat-sealing them in a plastic bag with 1 mL of the respective primary antibody dilution, as listed in Table 7. After overnight incubation, the membranes were washed three times for 10 min each with 1× TBST, then incubated with 10 mL of HRP-linked secondary antibody (anti-rabbit for arginase 2 and anti-mouse for β-actin and occludin), as listed in Table 7, for 1.5 hr, followed by three additional washes for 10 min each with 1× TBST.

Table 7: Primary and secondary antibody preparation for western blotting

Primary Antibodies	
β-Actin (1:2000)	Prepared in a ratio of 1:2000 with 2.5% BSA in 1x TBST
Arginase 2 (1:1000)	Prepared in a ratio of 1:1000 with 2.5% BSA in 1x TBST
Occludin (1:500)	Prepared in a ratio of 1:500 with 5% Nonfat Dried Milk Powder in 1x TBST
Secondary Antibodies	
Anti-Rabbit (1:5000)	Prepared in a ratio of 1:5000 with 2.5% BSA in 1x TBST
Anti-Mouse (1:5000)	Prepared in a ratio of 1:5000 with 2.5% BSA in 1x TBST

During the final wash step, the detection substrate was prepared at a 1:1 ratio using Bio-Rad's Clarity™ Western ECL Substrate. The substrate was pipetted into a tray; the membrane was placed face down on the substrate and incubated in the dark for 5 min before chemiluminescence detection using the ChemiDoc Imaging System. Densitometric measurements of the detected bands were performed using Bio-Rad's Image Lab 6.1 software, and the resulting values were normalized to -actin protein bands and used for analysis.

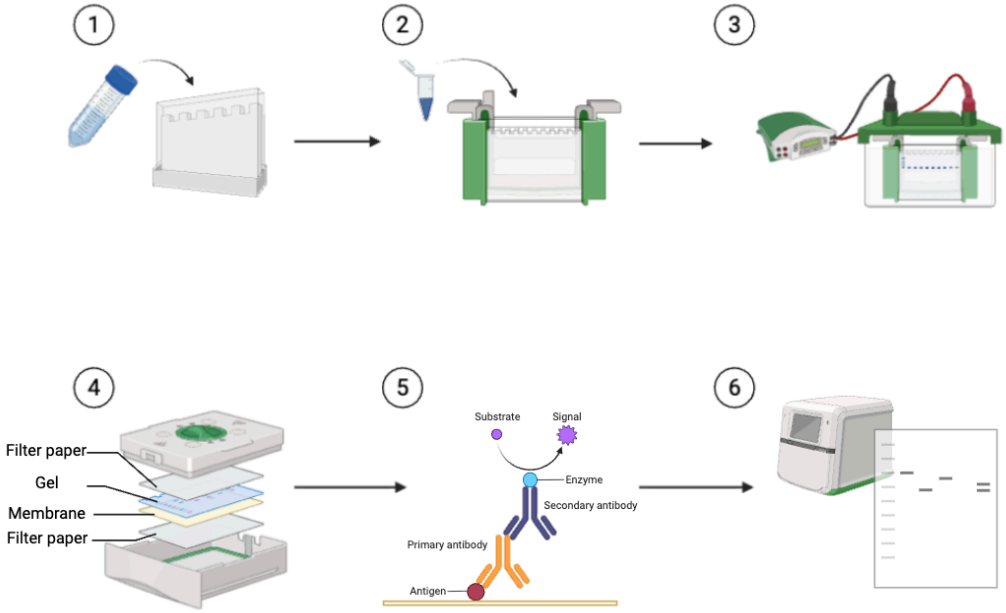

Figure 4: Western blot development flow chart. 1) *Gel casting* ***2)*** *Sample preparation* ***3)*** *SDS-PAGE* ***4)*** *Semi-dry protein transfer* ***5)*** *Incubation with primary and secondary antibodies, then treatment with substrate* ***6)*** *Detection and analysis. Created in BioRender.com.*

3.10 Tissue Preparation: Paraffin Embedding and Sectioning

Tissue paraffin embedding and sectioning were performed by a member of the working group, as described in Table 8. Briefly, tissue was collected from recently sacrificed mice, fixed in 4% PBS-buffered formaldehyde, rinsed, dehydrated, and embedded in paraffin. Freshly embedded samples were allowed to harden overnight at RT and were then sectioned into 4–5 µm slices using a microtome. Sections were mounted on glass slides and allowed to dry for three days before use in subsequent tissue staining procedures.

Table 8: Incubation steps for tissue paraffin embedding

Incubation Time	Solution
≥ 48 h	4% PBS buffered Formaldehyde
15 min	Rinse under cold running tap water
≥ 1 h	75% Ethanol

≥ 1 h	85% Ethanol
Overnight	95% Ethanol
≥ 1 h	100% Ethanol
≥ 1 h	100% Ethanol
≥ 1 h	100% Ethanol
30 min	100% Ethanol + Roti-Histol (1:1)
≥ 1 h	Roti-Histol I
≥ 1 h	Roti-Histol II
30 min	Paraffin I
30 min	Paraffin II
30 min	Paraffin III

3.11 Histological and Immunohistochemical Staining

Hematoxylin and Eosin (H&E) staining highlights morphological features and provides detailed structural information across different tissue types. Hematoxylin colors nucleic acids a deep blue-purple, while Eosin nonspecifically stains proteins pink, resulting in a clear contrast among nuclei, cytoplasm, and the extracellular matrix [77]. Meanwhile, Immunohistochemistry uses a series of steps, including antigen retrieval, primary antibody incubation, secondary antibody incubation, and the addition of a detection reagent, to localize and detect a target protein in cells and tissues [78].

H&E Staining

H&E staining was used to evaluate inflammatory characteristics in liver tissue from Arg2 KO and WT mice. H&E staining was performed using a series of rehydration, washing, and staining steps, as outlined in Table 9. Eosin counterstaining was applied by briefly coating the tissue (1-2 sec) with eosin, followed immediately by the dehydration steps.

Table 9: Steps for H&E staining

Solution	Time
Rehydration	

Roti-Histol	20 mins
100% EtOH	10 mins
95% EtOH	10 mins
85% EtOH	10 mins
70% EtOH	10 mins
30% EtOH	10 mins
Wash in ddH_2O	20 mins
Hematoxylin Staining	
Hematoxylin	20 sec
Tap Water 1	20 sec
Tap Water 2	10 sec
ddH_2O	Stop with distilled water
Wash in ddH_2O	10 mins
Dehydrogenation	
70% EtOH	8 mins
85% EtOH	8 mins
Eosin Counterstaining	
Dehydration	
95% EtOH	10 sec
100% EtOH	10 sec
Roti-Histol	20 mins
Entellan embedding and dried overnight under fume hood.	

Immunohistochemical Staining for Arginase 1 & 2 and Occludin

Immunohistochemical staining was used to identify and assess arginase 1, arginase 2, and occludin in small intestinal tissue, and arginase 1 in liver tissue from Arg2 KO and WT mice. For Arg1 & 2, tissue sections were deparaffinized, antigen retrieval performed, washed, outlined with a lipid pen, treated with 3% hydrogen peroxide, washed again, and blocked with 5% BSA in 1x TBST for 1 hr at RT (Table 10). For occludin, dewaxing and rehydration steps were performed, sections were outlined with a lipid pen and incubated with protease (Table 12). Following these initial steps, the remainder of the protocol was similar for all proteins.

The primary antibody was diluted as seen in Table 11. After removing the blocking solution, the primary antibody was applied to the tissue sections and incubated overnight at 4 °C in a humidified chamber. On the second day, slides were washed, and 30 min RT incubation in a humidified chamber with the HRP anti-rabbit secondary antibody (Table 11) was performed. DAB staining was performed by mixing 1 drop of DAB chromogen with 1 mL of DAB substrate. The solution was applied dropwise to the tissue sections and incubated for 1–10 min until a brown color developed. The reaction was then stopped by submerging the slides in ddH_2O. Slides were counterstained with hematoxylin, washed in ddH_2O, dehydrated, and mounted with a small drop of Entellan under a glass coverslip. Slides were then left to dry overnight before microscopic examination.

Table 10: Steps for immunohistochemical staining of Arginase 1 & 2

Solution	Time
Day 1	
Deparaffinization	
Roti-Histol	10 mins
100% EtOH	5 mins
96% EtOH	5 mins
70% EtOH	5 mins
Wash in ddH_2O	15 mins
Antigen Demasking	
10 mM Sodium Citrate	Heat until boiling then 30 min incubation at RT
Primary Antibody Incubation Preparation	
Incubate section in 3% Hydrogen Peroxide	10 mins at RT in a non-humidified chamber
Wash in ddH_2O	10 mins
Wash in 1x TBST	5 mins
Block sections with 5% BSA in 1x TBST	1 hour
Incubate sections with PA (1:1000)	Overnight at 4°C in humidified chamber
Day 2	

Wash in 1xTBST	15 mins
Incubate sections with SA (1:1)	30 mins at RT in humidified chamber
Wash in 1xTBST	15 mins
DAB Staining	
DAB Chromogen + Substrate mix (1 drop in 1 mL)	10 sec – 10 min
ddH_2O	Stop in distilled water
Hematoxylin Counterstaining	
Dehydration	
Wash in dH_2O	10 mins
70% EtOH	10 sec
96% EtOH	10 sec
100% EtOH	10 sec
Roti-Histol	10 mins
Entellan embedding and dried overnight under fume hood.	

Table 11: Antibody preparation for immunohistochemistry

Primary Antibodies	
Arginase 1 (1:1000)	Prepared in a ratio of 1:1000 with 5% BSA in 1x TBST
Arginase 2 (1:1000)	Prepared in a ratio of 1:1000 with 5% BSA in 1x TBST
Occludin (1:250)	Prepared in a ratio of 1:250 with 1xPBS
Secondary Antibodies	
Anti Rabbit (1:1)	Prepared in a ratio of 1:1 with 1x PBS.

Table 12: Steps for immunohistochemical staining of Occludin

Solution	**Time**
Day 1	
Dewaxing and Rehydration	

Roti-Histol	10 min
100% EtOH	5 min
96% EtOH	5 min
70% EtOH	5 min
dH2O	10 min
Protease Incubation	
Protease (2 mg/mL) in 1x PBS	10 min in 37 °C drying cabinet
Wash in 1xPBS	10 mins
PA (1:250) in 1xPBS	Overnight at 4 °C in humidified chamber
Day 2	
Wash in 1xPBS	9 mins
Incubate sections with SA (1:1)	30 mins at RT in humidified chamber
DAB Chromogen Staining	
Hematoxylin Counter Staining	
Dehydration	
70% EtOH	10 sec
96% EtOH	10 sec
100% EtOH	10 sec
Roti-Histol	10 mins

3.12 Triglyceride Determination via a Method Based on Folch Extraction in Tissue Samples

The simple method for the isolation and purification of total lipids from animal tissues was developed by Folch et al. and is now a widely used procedure for tissue lipid quantification [79,80]. In this method, tissue is homogenized in a 2:1 chloroform–methanol mixture and then washed with water or a salt solution, yielding a biphasic system in which the lower phase contains the total lipid fraction [80]. This phase is then collected and evaporated, and the resulting material can be quantified using a coupled enzymatic colorimetric assay. An adapted Folch et al. triglyceride extraction protocol was used to quantify triglyceride levels in liver tissue from Arg2 KO and WT mice.

Liver tissue (40-60 mg) was manually homogenized in 500 µL of ice-cold 2x PBS. An additional 500 µL of 2x PBS was added, and the samples were vortexed. Ultrasonic homogenization was performed in two 20-second cycles at 0.7 cycles and 100% amplitude, followed by vortexing. The homogenate was then divided into two equal volumes, 500 µL for triglyceride determination, and 500 µL for protein quantification (Section 3.8) after centrifugation at maximum speed for 5 mins at 4 °C.

For triglyceride analysis, samples were heated to 80 °C for 5 min on a mixing block and then cooled to RT. This was followed by the addition of 250 µL of methanol, vortexing, 5 min in an ultrasonic bath, and vortexing again. 500 µL of chloroform was then added, followed by vortexing and a 10 min ultrasonic bath. Samples were vortexed again and incubated for 2 hrs at RT, then centrifuged (max. speed, 5 min, 4 °C). 200 µL of the lower organic phase was transferred to a new Eppi and evaporated in a vacuum concentrator for 10 min. The dried lipid extract was resuspended in 200 µL of 5% BSA in dH_2O, heated for 10 min at 55 °C in a mixing block, and vortexed. Two cycles of ultrasonic homogenization (20 sec at 0.7 cycles and 100% amplitude) were performed, followed by heating at 55 °C for 1 hr. Samples were then stored overnight at −80 °C. The next day, the samples were reheated for 10 min at 55 °C on a mixing block, sonicated twice (20 sec at 0.7 cycles and 100% amplitude), and then heated again for 1 hr at 55 °C. Triglyceride measurement was performed using the TRIGs kit. 2 µL of standards, blanks (5% BSA in dH_2O), and samples were pipetted in triplicate into a 96-well plate. 200 µL of enzyme reagent was added to each well, and the plate was incubated for 10 min at 37 °C before being measured at 500 nm in the photometer.

3.13 Statistical Analysis

Data analysis and graphical representations were performed and prepared using GraphPad Prism 7.0. Outliers were identified using the Grubbs test and excluded if present. Normality of the data distribution was assessed using the Shapiro-Wilk test, and a one-sided unpaired t-test was used to evaluate statistical significance. All results are presented as mean ± standard error of the mean (SEM), and a p-value of ≤ 0.05 was considered statistically significant. For graphical representation,

values are expressed as the mean of knockout (KO) samples relative to the mean of wild-type (WT) samples, except for the NAFLD Activity Score (NAS), which is presented as absolute scores.

4. Results

4.1 Characteristics of Arg2 KO mice and wild-type animals

To determine if Arginase 2 was successfully knocked out in enterocyte-specific knockout mice, Arg2 protein expression in small intestinal tissue was assessed using Western blot and quantified relative to β-actin. As expected, Arg2 protein levels were not detectable in Arg2 KO mice. Staining for Arg2 in the small intestine (Fig. 5A) revealed clear Arg2 expression in the enterocytes of WT mice, whereas Arg2 staining was not detectable in the enterocytes of KO mice. In contrast, Arg1 was present in the small intestine of both WT and KO mice (Fig. 5B) and was also detected in liver tissue from both genotypes (Fig. 5C). Protein levels of Arg2 in WT and KO mice were further assessed by Western blot, which confirmed the absence of Arg2 protein in small intestinal tissue from KO mice (Fig. 5D). In addition, Arginase activity was measured to further validate the successful knockout of enterocyte-specific Arg2. Results revealed detectable activity in small intestinal tissue from WT mice and significantly reduced or non-detectable activity in tissue from KO mice (Fig. 5E). Meanwhile, nitrite levels, used as an indicator of NO production, did not differ between WT and KO mice (Fig. 5F).

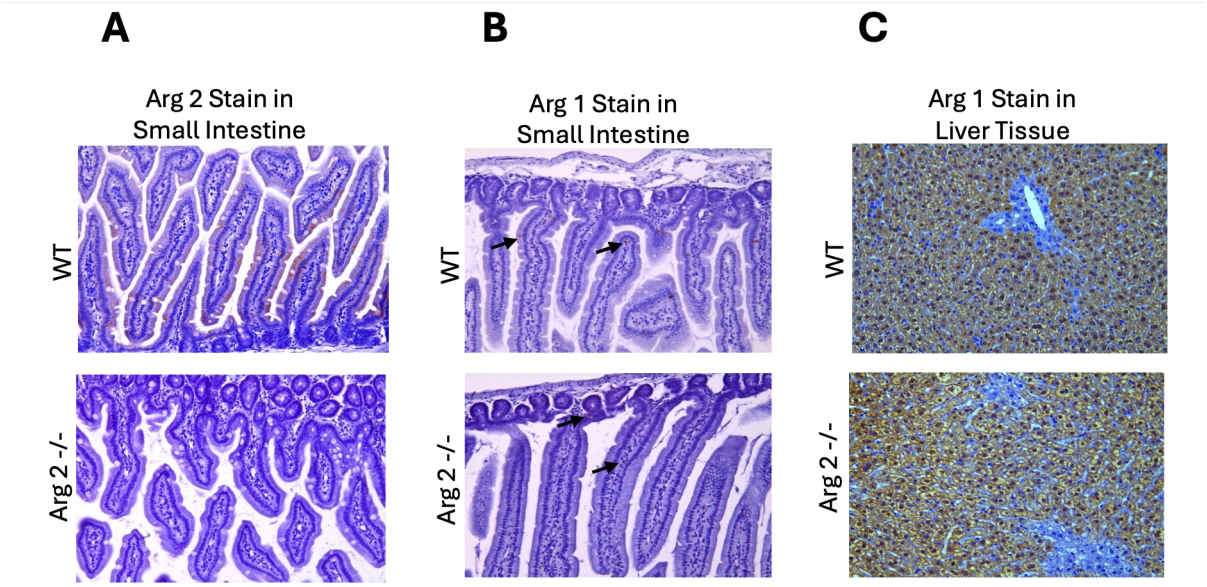

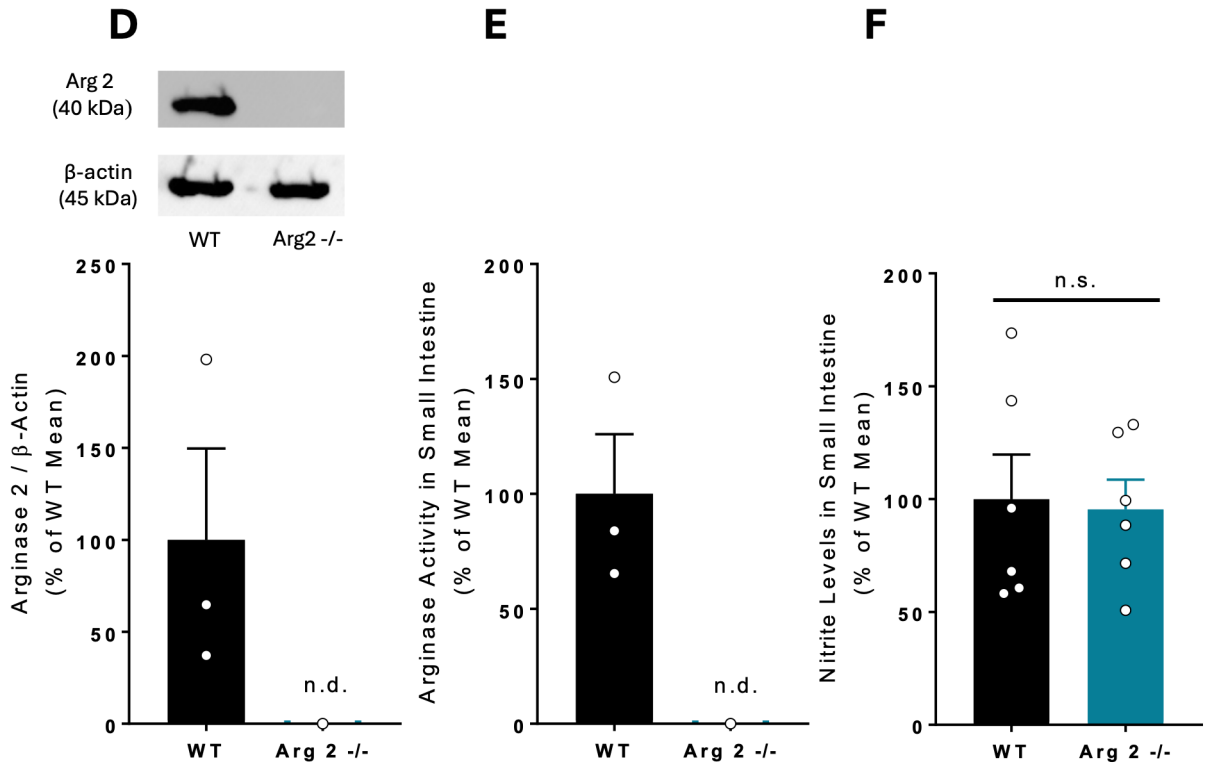

Figure 5: Characterization of the enterocyte-specific knock out of Arginase 2 in Arginase 2 knock out and wild type mice. A) *Representative images showing Arg2 protein expression in enterocytes of the small intestine from Arg2 WT and Arg KO mice. Magnification 200x.* ***B)*** *Representative images showing Arg1 protein expression in enterocytes of the small intestine from Arg2 WT and Arg KO mice. Magnification 200x.* ***C)*** *Representative images showing Arg1 protein expression in liver tissue of Arg2 WT and Arg KO mice. Magnification 200x.* ***D)*** *Protein levels of Arg2 in whole small intestinal tissue of Arg2 WT and Arg2 KO mice and representative western blot. Data are represented as mean ± SEM, n = 1-3, n.d. = not detectable.* ***E)*** *Arginase activity in small intestinal tissue of Arg2 WT and Arg KO mice. Data are represented as mean ± SEM, n = 3, n.d. = not detectable.* ***F)*** *Detection of nitrite as an indicator of NO in whole small intestinal tissue from Arg2 WT and Arg2 KO mice. Data are represented as mean ± SEM, n = 4-6, statistics performed with unpaired t-test, n.s. = not significant.*

4.2 Effect of a genetic deletion of Arg2 in enterocytes in liver histology and fat accumulation

As it has been shown before in feeding experiments that alteration of arginase activity in small intestinal tissue may be linked to MASLD development, liver tissue from Arg2 WT and Arg2 KO was examined for signs of inflammation. H&E staining revealed clear inflammatory foci in the liver tissue of KO mice compared to WT mice (Fig. 6A). Consistent with these observations, NAFLD activity scoring (NAS), a measure of liver inflammation, was significantly increased in KO mice compared to their WT counterparts (Fig. 6B). However, triglyceride measurements revealed no significant difference between the two groups (Fig. 6C).

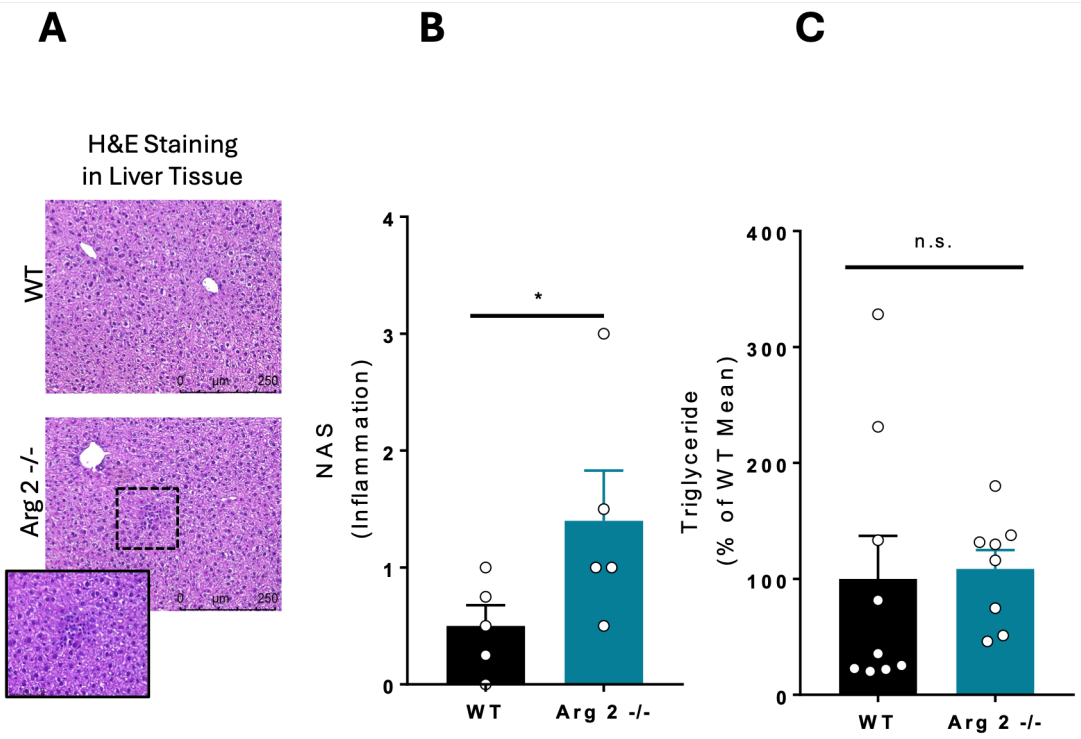

Figure 6: Assessment of inflammatory indices and triglyceride levels in the liver of enterocyte-specific Arginase 2 knock-out and wild-type mice. A) *H&E-stained representative images showing inflammatory foci in liver tissue from Arg2 WT and Arg2 KO mice. Magnification 200x and 600x.* ***B)*** *Evaluation of liver histology using NAFLD activity score (NAS) in Arg2 WT and Arg2 KO mice. Data are represented as mean ± SEM, n = 5, statistics performed with unpaired t-test (* = p ≤ 0.05).* ***C)*** *Triglyceride levels in Arg2 WT and Arg2 KO mice liver tissue. Data are represented as mean ± SEM, n = 8-9, statistics performed with unpaired t-test, n.s. = not significant.*

4.3 Effect of a genetic deletion of Arg2 in enterocytes on markers of permeability in small and large intestines

To determine if the enterocyte-specific knockdown of Arg2 was related to changes in tight junction protein levels, occludin protein levels, used as a marker of intestinal permeability, were determined by Western blot, quantified relative to β-actin, and in immunohistochemistry. Occludin protein levels were found to differ between Arg2 WT and Arg2 KO mice, with reduced levels in small intestinal tissue from KO mice compared to WT mice (Fig. 7A). Intestinal permeability was further evaluated in the small and large intestine using an ex vivo everted gut sac model. No statistically significant difference in permeability was observed in the small intestine between WT and KO mice (Fig. 7C). In contrast, colonic permeability was significantly increased in KO mice compared to WT mice (Fig. 7D).

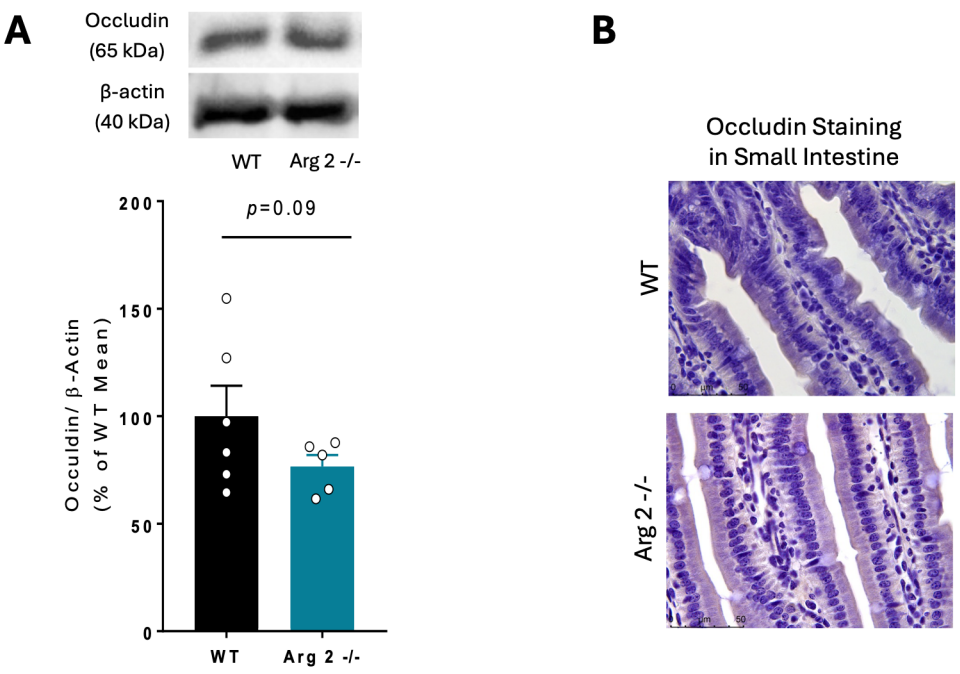

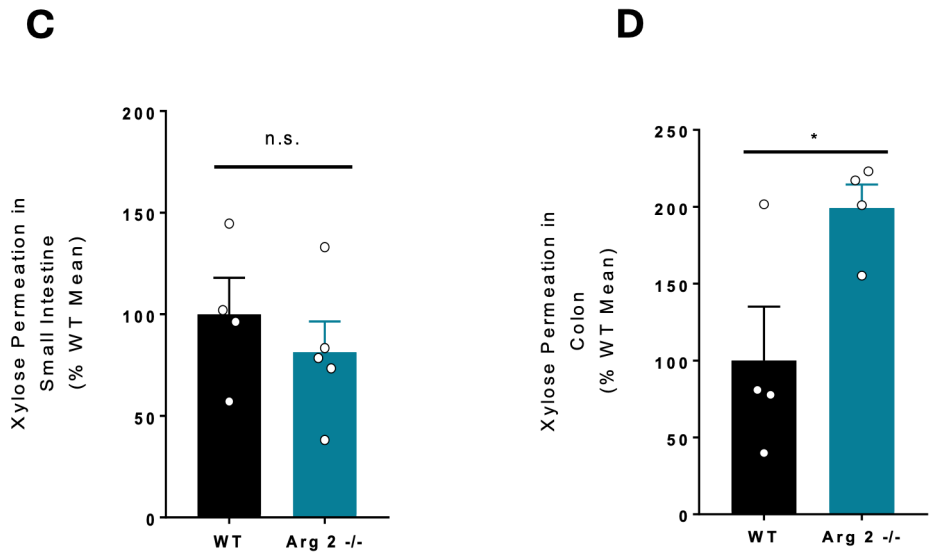

Figure 7: Small intestinal permeability assessed by occludin expression and xylose permeation in enterocyte-specific Arginase 2 knockout and wild-type mice. A) *Protein levels of occludin in small intestinal tissue of Arg2 WT and Arg2 KO mice compared to B-Actin (0.5 ug/uL) and representative western blot. Data are represented as mean ± SEM, n = 5-6, statistics performed with unpaired t-test, p = 0.09.* ***B)*** *Representative images showing occludin protein expression in small intestinal tissue of Arg2 WT and Arg KO mice. Magnification 600x. Xylose permeation in* ***C)*** *small intestinal tissue and* ***D)*** *colon tissue from Arg2 WT and Arg2 KO mice. Data are represented as mean ± SEM, n = 4–5, statistics performed with unpaired t-test, n.s. = not significant, * = p ≤ 0.05.*

5. Discussion

Over the past decades, increasing attention has been directed toward understanding the role of the intestinal barrier in human health and disease. Modifications in intestinal barrier function, especially changes in tight junction permeability, have been implicated in both the onset and progression of various diseases [1]. NO is a critical signaling molecule and homeostatic regulator of intestinal integrity through its effects on tight junctions [2], and has also been implicated in the development of different diseases, such as IBD and MASLD. However, the precise role of NO homeostasis in modulating intestinal permeability remains incompletely understood [43,81]. Therefore, this study aimed to determine whether an enterocyte-specific knockout of Arginase 2 affected NO homeostasis and, consequently, intestinal barrier permeability in mice.

5.1 Confirmation of a successful Arginase 2 genetic deletion in enterocytes of mice and characterization of the knockout

Arginase 2 has been identified as the primary arginase isoenzyme expressed in enterocytes of the small intestine [82,83] and has also been shown to be a critical homeostatic regulator of NOS expression and NO production [84]. In the present study, arginase 2 was selectively deleted in enterocytes of mice. As expected, Arg2 protein levels in the small intestines of knockout mice were undetectable (Fig. 5D). Measurements of arginase activity (Fig. 5E) and Arg2 staining of small intestinal tissue (Fig. 5A) also revealed undetectable levels of Arg2 in KO mice compared to WT mice. To confirm the specificity of the Arg2 knockout, Arg1 was stained in small-intestinal and liver tissues (Fig. 5B-C). A low but noticeable presence of Arg1 was observed in the small intestine, likely within the macrophages of this tissue, in both Arg2 KO and WT mice, while Arg1 staining in the liver tissue was pronounced throughout. Together, these results confirm the successful enterocyte-specific knockout of Arginase 2.

In theory, knockout of Arg2 should increase intracellular L-arginine availability, thereby enhancing substrate supply for inducible nitric oxide synthase (iNOS) and

promoting increased NO production. Previous studies have shown that the induction of arginase activity in immune stimulated IEC's reduces iNOS-derived NO, whereas pharmacological inhibition of arginase (e.g., nor-NOHA) increases NO production [43]. Similarly, reduced arginase activity in the small intestine has been associated with elevated nitrite levels in the context of MASLD [81]. Contrary to these expectations, no significant difference in nitrite levels was observed between Arg2 KO and WT mice (Fig. 5F).

A possible reason for this outcome is that NO was measured in whole small intestinal tissue rather than in isolated enterocytes; however, previous studies by our group have effectively demonstrated notable differences in NO levels within whole small intestinal tissue [81]. Lewis et al. and Nalepa et al. report that alterations in iNOS expression and NO production in Arg2-deficient models are often detectable only under conditions of infection or immune stimulation [85,86]. Thus, the lack of an inflammatory stimulus in our model may also explain why no significant differences in nitrite levels were observed under basal conditions. Furthermore, it cannot be ruled out that other compensatory mechanisms, such as Arginase 1 activity, are at play. Staining of Arg1 in the small intestine (Fig. 5B) was not quantified, but studies have shown that in the context of an Arg2 knockout and a Helicobacter pylori (*H. pylori*) infection, Arginase 1 gene expression and activity were significantly induced in gastric tissue and in bone marrow-derived macrophages [87], thereby depleting the cytosolic L-arg pool, decreasing substrate availability for iNOS, and reducing NO production [88].

In addition, methodological limitations may be considered. NO is highly reactive and short-lived, with rapid membrane diffusion and a broad physiological concentration range, making accurate quantification inherently challenging [89,90]. The Griess reaction assay measures nitrite as an indirect indicator of NO in biological samples. In this assay, nitrate must be reduced to nitrite, either chemically or enzymatically, to determine nitrite levels. However, the nitrate-to-nitrite conversion is not specific, and nitrite can be further reduced to NO, leading to an underestimation of nitrite in samples [91,92].

Future research should include NO level measurements in whole small intestinal tissue and isolated enterocytes, alongside assessments of iNOS mRNA and protein expression. Examining pro-inflammatory cytokines that influence iNOS activity and exploring compensatory mechanisms, such as Arg1 expression, could offer a more comprehensive understanding of basal NO homeostasis in these enterocyte-specific Arg2 knockout mice.

5.2 The physiological effects of an enterocyte-specific knockout of Arginase 2 on the liver and the intestines

Systemic Arg2 deficiency has been implicated in the development of spontaneous hepatic inflammation and steatosis [93], both under basal conditions of the knockout and during exacerbation of diet-induced liver damage [93,94]. Consistent with this, we observed clear inflammatory foci in the livers of Arg2 KO mice, along with significantly higher NAS inflammation scores compared to WT controls (Fig.6A-B). However, hepatic triglyceride levels did not differ between groups (Fig.6C).

Considering studies have shown Arg2 to be expressed in macrophages and that its systemic deficiency promotes pro-inflammatory activation of Kupffer cells [93], leading to spontaneous liver inflammation and fat buildup [95], one might expect increased triglyceride accumulation in Arg2 KO mice. In contrast, Liu et al. reported that a systemic Arg2 knockdown reduced inflammatory cytokine and macrophage infiltration in the liver. They also reported significantly less hepatic steatosis, decreased triglyceride levels, and reduced expression and activity of hepatic lipogenic regulators, thereby mitigating de novo lipogenesis in the liver in Arg2 KO mice [96].

Liver inflammation observed in the Arg2 KO mice could also be linked to alterations in tight junction proteins. Given the bidirectional communication between the intestine and liver via the portal circulation and hepatic bile flow, it remains unclear whether changes in tight junctions and increased gut permeability are causes or consequences of liver damage [97]. Nevertheless, even if increased intestinal permeability is not a primary driver of disease initiation, it likely contributes to disease progression and systemic inflammation [35,98]. In conjunction with the

elevated inflammatory foci and increased NAS scores observed in the livers of Arg2 KO mice, we detected reduced occludin protein levels in the small intestine of Arg2 KO mice (Fig.7A).

Occludin is a key tight junction protein that regulates intermembrane and paracellular diffusion of small molecules in the intestinal barrier [99,100]. It also plays a critical role in maintaining tissue integrity and intestinal barrier function [81]. Reduced expression of occludin and claudin-1 has been reported in the intestinal epithelium of patients with liver disease [101,102]. Both experimental and clinical studies indicate that intestinal barrier dysfunction and increased gut permeability can exacerbate liver pathology, in part by promoting systemic endotoxemia [102–104]. In systemic Arg2 knockout models, tight junction proteins are affected by both reduced polyamine production and increased reactive oxygen and nitrosative species, thereby increasing intestinal barrier permeability [105,106]. In contrast, although tight junction protein levels were reduced in the small intestines of our KO mice, no significant differences in small-intestinal permeability were observed (Fig.7C). Notably, a significant difference in large-intestinal permeability was observed between Arg2 KO and WT mice (Fig.7D).

Altered arginine metabolism has been proposed as a potential biomarker of IBD progression [57]. IBD, including ulcerative colitis (UC) and Crohn's disease [107], is characterized by chronic inflammation and increased intestinal permeability, particularly in the large intestine [108,109]. In a DSS-induced colitis model, systemic Arg2 knockout increased susceptibility to colitis and enhanced oxidative stress in intestinal organoids. The authors proposed that increased intestinal permeability in these mice was linked to Arg2's role in spermidine synthesis and IL-10 signaling in inflammatory macrophages. Given that spermidine modulates ROS and IL-10 signaling supports an anti-inflammatory phenotype, the loss of Arg2 was suggested to promote a pro-inflammatory shift in immune cells, and that this shift, rather than enhanced NO production, accounted for the increased permeability observed in the large intestine [105]. However, Arg1 has also been implicated in the pathogenesis of IBD. It also metabolizes L-arg into ornithine, a precursor for polyamine and proline synthesis, thereby helping protect cells from oxidative damage caused by ROS

[110]. Studies have demonstrated a link between the level of inflammation in IBD patients and Arg1 mRNA expression [111]. Increased Arg1 and iNOS expression and activity have also been reported in various experimental colitis murine models and in the submucosal tissues of IBD patients. However, this study suggests that Arg1 may influence intestinal permeability by regulating L-arg availability and altering the intestinal microbiota, thereby increasing permeability and exacerbating IBD [112]. In the current enterocyte-specific Arg2 knockout model, increased large-intestinal permeability was observed, but it is unclear whether Arg1 expression or activity was affected. This could indicate a potential compensatory mechanism that warrants further investigation.

Conversely, increased iNOS expression and NO production have long been associated with colitis and IBD [113,114]. Studies using Arg2 KO mice and Arg2 KO gastric macrophage cell models during acute *H. pylori* infection demonstrated that Arg2 expression can restrict NO production either by competing with iNOS for L-arg or by contributing to polyamine production. Although inhibition of arginases or ODC can both increase iNOS protein synthesis, this study indicates that increased L-arg availability for iNOS is ultimately responsible for increased iNOS functional activity and thus NO production [86]. These findings highlight the complex interplay between arginine metabolism, polyamine synthesis, and NO signaling. In the context of our model, it remains unclear whether the increased large-intestinal permeability is driven predominantly by altered L-arg availability and metabolism, NO levels and tight-junction integrity, disrupted polyamine production, or immune-mediated mechanisms.

Taken together, these findings suggest that enterocyte-specific deletion of Arginase 2 is associated with altered levels of tight junction proteins, increased intestinal permeability, and liver inflammation. While these results partially support our initial hypothesis, important limitations, including sample size, sex, and age of the animals, should be considered. Further studies incorporating inflammatory challenges and more detailed molecular analyses will be necessary to clarify how an Arg2 deletion in enterocytes influences nitric oxide homeostasis and intestinal barrier function.

6. Conclusion

With the increasing prevalence of intestinal barrier–related diseases, particularly leaky gut, understanding the mechanisms that regulate epithelial integrity is of growing importance. This would not only advance our understanding of disease pathogenesis but also inform the development of novel therapeutic strategies and support the progression of personalized medicine.

In this study, an investigation of an enterocyte-specific Arg2 knockout mouse model revealed reduced tight-junction levels in small-intestinal tissue, increased intestinal permeability in the large intestine, and signs of liver inflammation, with no significant changes in nitrite levels in small intestinal tissue. Together, these findings suggest that Arg2 in the small intestine of young mice contributes to the regulation of the intestinal epithelial barrier and may be involved in liver inflammatory responses. However, the mechanisms by which Arg2 and nitric oxide homeostasis contribute to these changes remain unclear.

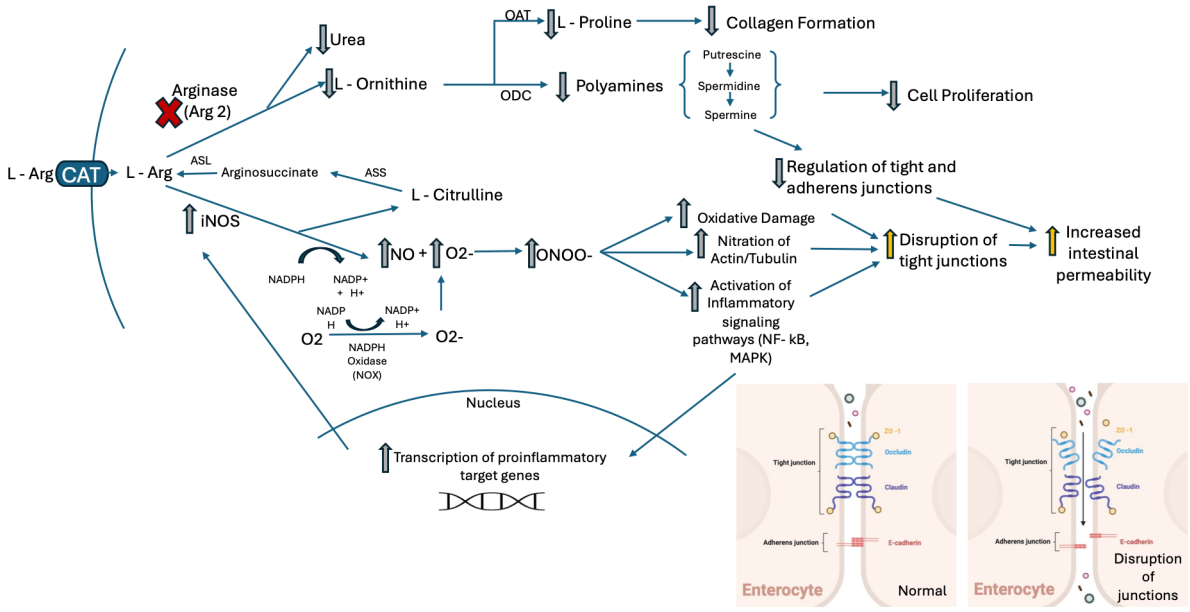

Figure 8: Schematic depiction of the possible effects of knocking down Arg2 in enterocytes. *L-arg is transported into IECs by CATs. In Arg2 KO mice, excess L-arg is redirected toward iNOS, increasing NO and ONOO⁻ production. This promotes oxidative damage, cytoskeletal protein nitration, and inflammatory signaling, which*

together disrupt tight and adherens junctions. Reduced Arg2-dependent polyamine synthesis further destabilizes junctional proteins, thereby increasing intestinal permeability. Legend: OAT = ornithine aminotransferase, ODC = ornithine decarboxylase, ASS = argininosuccinate synthetase, ASL = argininosuccinate lyase, red markings: successfully shown in current work, yellow markings: partially shown in current work, grey markings: not shown in current work.

Current literature underscores that the Arg–NO pathway is regulated by multiple interacting factors, including L-arginine transport, cellular enzyme localization, immune activation, and endotoxin exposure. As a result, this pathway should not be seen as a simplified model of two enzymes competing for the same substrate. Instead, the relationship between Arg2 activity and nitric oxide homeostasis appears to be context-dependent and multifactorial. Further investigation of how nitric oxide is regulated and signaled in this specific knockout model is important to understanding the connection between Arg2 deficiency, barrier dysfunction, systemic inflammation, and disease progression.

References

1. Turner JR. Intestinal mucosal barrier function in health and disease. Nat Rev Immunol. 2009;9: 799–809. doi:10.1038/nri2653

2. Rao JN, Wang J-Y. Intestinal Architecture and Development. Regulation of Gastrointestinal Mucosal Growth. Morgan & Claypool Life Sciences; 2010. Available: https://www.ncbi.nlm.nih.gov/books/NBK54098/

3. Collins JT, Nguyen A, Omole AE, Badireddy M. Anatomy, Abdomen and Pelvis, Small Intestine. StatPearls. Treasure Island (FL): StatPearls Publishing; 2025. Available: http://www.ncbi.nlm.nih.gov/books/NBK459366/

4. Darwich AS, Aslam U, Ashcroft DM, Rostami-Hodjegan A. Meta-Analysis of the Turnover of Intestinal Epithelia in Preclinical Animal Species and Humans. Drug Metab Dispos. 2014;42: 2016–2022. doi:10.1124/dmd.114.058404

5. Neurath MF, Artis D, Becker C. The intestinal barrier: a pivotal role in health, inflammation, and cancer. Lancet Gastroenterol Hepatol. 2025;10: 573–592. doi:10.1016/S2468-1253(24)00390-X

6. Luissint A-C, Parkos CA, Nusrat A. Inflammation and the Intestinal Barrier: Leukocyte–Epithelial Cell Interactions, Cell Junction Remodeling, and Mucosal Repair. Gastroenterology. 2016;151: 616–632. doi:10.1053/j.gastro.2016.07.008

7. Ogobuiro I, Gonzales J, Shumway KR, Tuma F. Physiology, Gastrointestinal. StatPearls. Treasure Island (FL): StatPearls Publishing; 2025. Available: http://www.ncbi.nlm.nih.gov/books/NBK537103/

8. Azzouz LL, Sharma S. Physiology, Large Intestine. StatPearls. Treasure Island (FL): StatPearls Publishing; 2025. Available: http://www.ncbi.nlm.nih.gov/books/NBK507857/

9. Kong S, Zhang YH, Zhang W. Regulation of Intestinal Epithelial Cells Properties and Functions by Amino Acids. BioMed Res Int. 2018;2018: 2819154. doi:10.1155/2018/2819154

10. Higa T, Okita Y, Matsumoto A, Nakayama S, Oka T, Sugahara O, et al. Spatiotemporal reprogramming of differentiated cells underlies regeneration and neoplasia in the intestinal epithelium. Nat Commun. 2022;13: 1500. doi:10.1038/s41467-022-29165-z

11. Untersmayr E, Brandt A, Koidl L, Bergheim I. The Intestinal Barrier Dysfunction as Driving Factor of Inflammaging. Nutrients. 2022;14: 949. doi:10.3390/nu14050949

12. Okumura R, Takeda K. Roles of intestinal epithelial cells in the maintenance of gut homeostasis. Exp Mol Med. 2017;49: e338–e338. doi:10.1038/emm.2017.20

13. Sluis MV der, Koning BAED, Bruijn ACJMD, Velcich A, Meijerink JPP, Goudoever JBV, et al. Muc2-Deficient Mice Spontaneously Develop Colitis, Indicating That MUC2 Is Critical for Colonic Protection. Gastroenterology. 2006;131: 117–129. doi:10.1053/j.gastro.2006.04.020

14. Lei H, Yu D, Xue Y-B, Li Y-H, Gong S-M, Peng Y-Y, et al. Tuft cells utilize taste signaling molecules to respond to the pathobiont microbe Ruminococcus gnavus in the proximal colon. Front Immunol. 2023;14: 1259521. doi:10.3389/fimmu.2023.1259521

15. Gwak M-G, Chang S-Y. Gut-Brain Connection: Microbiome, Gut Barrier, and Environmental Sensors. Immune Netw. 2021;21: e20. doi:10.4110/in.2021.21.e20

16. Umar S. Intestinal Stem Cells. Curr Gastroenterol Rep. 2010;12: 340–348. doi:10.1007/s11894-010-0130-3

17. Sauls RS, Taylor BN. Histology, M Cell. StatPearls. Treasure Island (FL): StatPearls Publishing; 2025. Available: http://www.ncbi.nlm.nih.gov/books/NBK534232/

18. Dillon A, Lo DD. M Cells: Intelligent Engineering of Mucosal Immune Surveillance. Front Immunol. 2019;10. doi:10.3389/fimmu.2019.01499

19. Malagola E, Vasciaveo A, Ochiai Y, Kim W, Zheng B, Zanella L, et al. Isthmus progenitor cells contribute to homeostatic cellular turnover and support regeneration following intestinal injury. Cell. 2024;187: 3056-3071.e17. doi:10.1016/j.cell.2024.05.004

20. Ali A, Tan H, Kaiko GE. Role of the Intestinal Epithelium and Its Interaction With the Microbiota in Food Allergy. Front Immunol. 2020;11: 604054. doi:10.3389/fimmu.2020.604054

21. Swidsinski A, Weber J, Loening-Baucke V, Hale LP, Lochs H. Spatial Organization and Composition of the Mucosal Flora in Patients with Inflammatory Bowel Disease. J Clin Microbiol. 2005;43: 3380–3389. doi:10.1128/JCM.43.7.3380-3389.2005

22. Johansson MEV, Phillipson M, Petersson J, Velcich A, Holm L, Hansson GC. The inner of the two Muc2 mucin-dependent mucus layers in colon is devoid of bacteria. Proc Natl Acad Sci. 2008;105: 15064–15069. doi:10.1073/pnas.0803124105

23. Jensen BAH, Heyndrickx M, Jonkers D, Mackie A, Millet S, Naghibi M, et al. Small intestine vs. colon ecology and physiology: Why it matters in probiotic

administration. Cell Rep Med. 2023;4: 101190. doi:10.1016/j.xcrm.2023.101190

24. Macura B, Kiecka A, Szczepanik M. Intestinal permeability disturbances: causes, diseases and therapy. Clin Exp Med. 2024;24: 232. doi:10.1007/s10238-024-01496-9

25. Lee W, Kim J, Lim S-S, Kim Y, Ahn Y-S, Yoon J-H. External Airborne-agent Exposure Increase Risk of Digestive Tract Cancer. Sci Rep. 2020;10: 8617. doi:10.1038/s41598-020-65312-6

26. Celebi Sozener Z, Ozdel Ozturk B, Cerci P, Turk M, Gorgulu Akin B, Akdis M, et al. Epithelial barrier hypothesis: Effect of the external exposome on the microbiome and epithelial barriers in allergic disease. Allergy. 2022;77: 1418–1449. doi:10.1111/all.15240

27. Akdis CA. Does the epithelial barrier hypothesis explain the increase in allergy, autoimmunity and other chronic conditions? Nat Rev Immunol. 2021;21: 739–751. doi:10.1038/s41577-021-00538-7

28. Odenwald MA, Turner JR. The intestinal epithelial barrier: a therapeutic target? Nat Rev Gastroenterol Hepatol. 2017;14: 9–21. doi:10.1038/nrgastro.2016.169

29. Samadi N, Klems M, Untersmayr E. The role of gastrointestinal permeability in food allergy. Ann Allergy Asthma Immunol. 2018;121: 168–173. doi:10.1016/j.anai.2018.05.010

30. König J, Wells J, Cani PD, García-Ródenas CL, MacDonald T, Mercenier A, et al. Human Intestinal Barrier Function in Health and Disease. Clin Transl Gastroenterol. 2016;7: e196. doi:10.1038/ctg.2016.54

31. Le NPK, Altenburger MJ, Lamy E. Development of an Inflammation-Triggered In Vitro “Leaky Gut” Model Using Caco-2/HT29-MTX-E12 Combined with Macrophage-like THP-1 Cells or Primary Human-Derived Macrophages. Int J Mol Sci. 2023;24: 7427. doi:10.3390/ijms24087427

32. Mu K, Yu S, Kitts DD, Mu K, Yu S, Kitts DD. The Role of Nitric Oxide in Regulating Intestinal Redox Status and Intestinal Epithelial Cell Functionality. Int J Mol Sci. 2019;20. doi:10.3390/ijms20071755

33. Monaco A, Ovryn B, Axis J, Amsler K. The Epithelial Cell Leak Pathway. Int J Mol Sci. 2021;22: 7677. doi:10.3390/ijms22147677

34. Di Tommaso N, Gasbarrini A, Ponziani FR. Intestinal Barrier in Human Health and Disease. Int J Environ Res Public Health. 2021;18: 12836. doi:10.3390/ijerph182312836

35. Chopyk DM, Grakoui A. Contribution of the Intestinal Microbiome and Gut Barrier to Hepatic Disorders. Gastroenterology. 2020;159: 849–863. doi:10.1053/j.gastro.2020.04.077

36. Lessey LR, Robinson SC, Chaudhary R, Daniel JM. Adherens junction proteins on the move—From the membrane to the nucleus in intestinal diseases. Front Cell Dev Biol. 2022;10: 998373. doi:10.3389/fcell.2022.998373

37. Uematsu S, Fujimoto K, Jang MH, Yang B-G, Jung Y-J, Nishiyama M, et al. Regulation of humoral and cellular gut immunity by lamina propria dendritic cells expressing Toll-like receptor 5. Nat Immunol. 2008;9: 769–776. doi:10.1038/ni.1622

38. Surd AO, Răducu C, Răducu E, Ihuț A, Munteanu C. Lamina Propria and GALT: Their Relationship with Different Gastrointestinal Diseases, Including Cancer. Gastrointest Disord. 2024;6: 947–963. doi:10.3390/gidisord6040066

39. Mu Q, Kirby J, Reilly CM, Luo XM. Leaky Gut As a Danger Signal for Autoimmune Diseases. Front Immunol. 2017;8: 598. doi:10.3389/fimmu.2017.00598

40. Kinnebrew MA, Pamer EG. Innate immune signaling in defense against intestinal microbes. Immunol Rev. 2012;245: 113–131. doi:10.1111/j.1600-065X.2011.01081.x

41. Hartwig O, Loretz B, Nougarede A, Jary D, Sulpice E, Gidrol X, et al. Leaky gut model of the human intestinal mucosa for testing siRNA-based nanomedicine targeting JAK1. J Controlled Release. 2022;345: 646–660. doi:10.1016/j.jconrel.2022.03.037

42. Brandt A, Baumann A, Hernández-Arriaga A, Jung F, Nier A, Staltner R, et al. Impairments of intestinal arginine and NO metabolisms trigger aging-associated intestinal barrier dysfunction and 'inflammaging'. Redox Biol. 2022;58: 102528. doi:10.1016/j.redox.2022.102528

43. Talavera MM, Nuthakki S, Cui H, Jin Y, Liu Y, Nelin LD. Immunostimulated Arginase II Expression in Intestinal Epithelial Cells Reduces Nitric Oxide Production and Apoptosis. Front Cell Dev Biol. 2017;5. doi:10.3389/fcell.2017.00015

44. Abu-Soud HM, Stuehr DJ. Nitric oxide synthases reveal a role for calmodulin in controlling electron transfer. Proc Natl Acad Sci U S A. 1993;90: 10769–10772. doi:10.1073/pnas.90.22.10769

45. Cinelli MA, Do HT, Miley GP, Silverman RB. Inducible Nitric Oxide Synthase: Regulation, Structure, and Inhibition. Med Res Rev. 2020;40: 158–189. doi:10.1002/med.21599

46. Pautz A, Art J, Hahn S, Nowag S, Voss C, Kleinert H. Regulation of the expression of inducible nitric oxide synthase. Nitric Oxide. 2010;23: 75–93. doi:10.1016/j.niox.2010.04.007

47. Zhou X, Yang W, Li J. Ca2+- and Protein Kinase C-dependent Signaling Pathway for Nuclear Factor-κB Activation, Inducible Nitric-oxide Synthase Expression, and Tumor Necrosis Factor-α Production in Lipopolysaccharide-stimulated Rat Peritoneal Macrophages *. J Biol Chem. 2006;281: 31337–31347. doi:10.1016/S0021-9258(19)84046-2

48. Baier J, Gänsbauer M, Giessler C, Arnold H, Muske M, Schleicher U, et al. Arginase impedes the resolution of colitis by altering the microbiome and metabolome. J Clin Invest. 2020;130. doi:10.1172/JCI126923

49. Koo B-H, Won M-H, Kim Y-M, Ryoo S. p32-Dependent p38 MAPK Activation by Arginase II Downregulation Contributes to Endothelial Nitric Oxide Synthase Activation in HUVECs. Cells. 2020;9: 392. doi:10.3390/cells9020392

50. Singh K, Coburn LA, Barry DP, Boucher J-L, Chaturvedi R, Wilson KT. L-arginine uptake by cationic amino acid transporter 2 is essential for colonic epithelial cell restitution. Am J Physiol - Gastrointest Liver Physiol. 2012;302: G1061–G1073. doi:10.1152/ajpgi.00544.2011

51. Canè S, Geiger R, Bronte V. The roles of arginases and arginine in immunity. Nat Rev Immunol. 2025;25: 266–284. doi:10.1038/s41577-024-01098-2

52. Tsoukias NM, Kavdia M, Popel AS. A theoretical model of nitric oxide transport in arterioles: frequency- vs. amplitude-dependent control of cGMP formation. Am J Physiol-Heart Circ Physiol. 2004;286: H1043–H1056. doi:10.1152/ajpheart.00525.2003

53. Wise DL, Houghton G. Diffusion coefficients of neon, krypton, xenon, carbon monoxide and nitric oxide in water at 10–60°C. Chem Eng Sci. 1968;23: 1211–1216. doi:10.1016/0009-2509(68)89029-3

54. Pacher P, Beckman JS, Liaudet L. Nitric Oxide and Peroxynitrite in Health and Disease. Physiol Rev. 2007;87: 315–424. doi:10.1152/physrev.00029.2006

55. Rath M, Müller I, Kropf P, Closs EI, Munder M. Metabolism via Arginase or Nitric Oxide Synthase: Two Competing Arginine Pathways in Macrophages. Front Immunol. 2014;5: 532. doi:10.3389/fimmu.2014.00532

56. Beckman JS, Koppenol WH. Nitric oxide, superoxide, and peroxynitrite: the good, the bad, and ugly. Am J Physiol. 1996;271: C1424-1437. doi:10.1152/ajpcell.1996.271.5.C1424

57. Li J-Y, Guo Y-C, Zhou H-F, Yue T-T, Wang F-X, Sun F, et al. Arginine metabolism regulates the pathogenesis of inflammatory bowel disease. Nutr Rev. 2023;81: 578–586. doi:10.1093/nutrit/nuac070

58. Katsube T, Tsuji H, Onoda M. Nitric oxide attenuates hydrogen peroxide-induced barrier disruption and protein tyrosine phosphorylation in monolayers of intestinal epithelial cell. Biochim Biophys Acta BBA - Mol Cell Res. 2007;1773: 794–803. doi:10.1016/j.bbamcr.2007.03.002

59. Schopfer FJ, Baker PRS, Freeman BA. NO-dependent protein nitration: a cell signaling event or an oxidative inflammatory response? Trends Biochem Sci. 2003;28: 646–654. doi:10.1016/j.tibs.2003.10.006

60. Niu F, Yu Y, Li Z, Ren Y, Li Z, Ye Q, et al. Arginase: An emerging and promising therapeutic target for cancer treatment. Biomed Pharmacother. 2022;149: 112840. doi:10.1016/j.biopha.2022.112840

61. Mirmiran P, Moghadam SK, Bahadoran Z, Ghasemi A, Azizi F. Dietary L-Arginine Intakes and the Risk of Metabolic Syndrome: A 6-Year Follow-Up in Tehran Lipid and Glucose Study. Prev Nutr Food Sci. 2017;22: 263–270. doi:10.3746/pnf.2017.22.4.263

62. Xu W, Asosingh K, Janocha AJ, Madden E, Wanner N, Trotter D, et al. Mitochondrial arginase 2 regulates hematopoietic and cardiovascular adaptation to hypoxia. Blood Vessels Thromb Hemost. 2025;3: 100110. doi:10.1016/j.bvth.2025.100110

63. Ansermet C, Centeno G, Lagarrigue S, Nikolaeva S, Yoshihara HA, Pradervand S, et al. Renal tubular arginase-2 participates in the formation of the corticomedullary urea gradient and attenuates kidney damage in ischemia-reperfusion injury in mice. Acta Physiol. 2020;229: e13457. doi:10.1111/apha.13457

64. Verhoeckx K, Cotter P, López-Expósito I, Kleiveland C, Lea T, Mackie A, et al. In Vitro Intestinal Tissue Models: General Introduction. The Impact of Food Bioactives on Health: in vitro and ex vivo models [Internet]. Springer; 2015. Available: https://www.ncbi.nlm.nih.gov/books/NBK500171/

65. Hamilton KL, Butt AG. Glucose transport into everted sacs of the small intestine of mice. Adv Physiol Educ. 2013;37: 415–426. doi:10.1152/advan.00017.2013

66. Eberts TJ, Sample RH, Glick MR, Ellis GH. A simplified, colorimetric micromethod for xylose in serum or urine, with phloroglucinol. Clin Chem. 1979;25: 1440–1443.

67. Hermida C, Martínez-Costa OH, Corrales G, Teruel C, Sánchez V, Sánchez JJ, et al. Improvement and Validation of d-Xylose Determination in Urine and Serum as a New Tool for the Noninvasive Evaluation of Lactase Activity in Humans. J Clin Lab Anal. 2014;28: 478–486. doi:10.1002/jcla.21713

68. Hayashi M, Hirose H, Senga S, Onitsuka A, Fuwa S, Mori Y, et al. Effect of portal hypertension caused by chronic high venous pressure on small-intestinal sugar absorption. Nutrition. 2000;16: 30–33. doi:10.1016/S0899-9007(99)00187-2

69. Griess Reagent System. [cited 15 Dec 2025]. Available: https://at.promega.com/products/cell-health-assays/oxidative-stress-assays/griess-reagent-system/

70. Corraliza IM, Campo ML, Soler G, Modolell M. Determination of arginase activity in macrophages: a micromethod. J Immunol Methods. 1994;174: 231–235. doi:10.1016/0022-1759(94)90027-2

71. Chomczynski P, Sacchi N. Single-step method of RNA isolation by acid guanidinium thiocyanate-phenol-chloroform extraction. Anal Biochem. 1987;162: 156–159. doi:10.1006/abio.1987.9999

72. Rio DC, Ares M, Hannon GJ, Nilsen TW. Purification of RNA using TRIzol (TRI reagent). Cold Spring Harb Protoc. 2010;2010: pdb.prot5439. doi:10.1101/pdb.prot5439

73. Wingfield PT. Use of Protein Folding Reagents. Curr Protoc Protein Sci Editor Board John E Coligan Al. 2001;APPENDIX 3: Appendix-3A. doi:10.1002/0471140864.psa03as00

74. Bradford MM. A rapid and sensitive method for the quantitation of microgram quantities of protein utilizing the principle of protein-dye binding. Anal Biochem. 1976;72: 248–254. doi:10.1016/0003-2697(76)90527-3

75. Kielkopf CL, Bauer W, Urbatsch IL. Bradford Assay for Determining Protein Concentration. Cold Spring Harb Protoc. 2020;2020: 102269. doi:10.1101/pdb.prot102269

76. Hidayat R, Wulandari P. Western Blotting (WB) Technique Guideline for Separation and Isolation of Protein. Biosci Med J Biomed Transl Res. 2021;5: 367–380. doi:10.37275/bsm.v5i4.229

77. Fischer AH, Jacobson KA, Rose J, Zeller R. Hematoxylin and eosin staining of tissue and cell sections. CSH Protoc. 2008;2008: pdb.prot4986. doi:10.1101/pdb.prot4986

78. Magaki S, Hojat SA, Wei B, So A, Yong WH. An Introduction to the Performance of Immunohistochemistry. Methods Mol Biol Clifton NJ. 2019;1897: 289–298. doi:10.1007/978-1-4939-8935-5_25

79. Mopuri R, Kalyesubula M, Rosov A, Edery N, Moallem U, Dvir H. Improved Folch Method for Liver-Fat Quantification. Front Vet Sci. 2021;7: 594853. doi:10.3389/fvets.2020.594853

80. Folch J, Lees M, Sloane Stanley GH. A simple method for the isolation and purification of total lipides from animal tissues. J Biol Chem. 1957;226: 497–509.

81. Baumann A, Rajcic D, Brandt A, Sánchez V, Jung F, Staltner R, et al. Alterations of nitric oxide homeostasis as trigger of intestinal barrier dysfunction in non-alcoholic fatty liver disease. J Cell Mol Med. 2022;26: 1206–1218. doi:10.1111/jcmm.17175

82. Ozaki M, Gotoh T, Nagasaki A, Miyanaka K, Takeya M, Fujiyama S, et al. Expression of Arginase II and Related Enzymes in the Rat Small Intestine and Kidney1. J Biochem (Tokyo). 1999;125: 586–593. doi:10.1093/oxfordjournals.jbchem.a022324

83. Köhler ES, Sankaranarayanan S, van Ginneken CJ, van Dijk P, Vermeulen JL, Ruijter JM, et al. The human neonatal small intestine has the potential for arginine synthesis; developmental changes in the expression of arginine-synthesizing and -catabolizing enzymes. BMC Dev Biol. 2008;8: 107. doi:10.1186/1471-213X-8-107

84. Durante W, Johnson FK, Johnson RA. Arginase: A Critical Regulator of Nitric Oxide Synthesis and Vascular Function. Clin Exp Pharmacol Physiol. 2007;34: 906–911. doi:10.1111/j.1440-1681.2007.04638.x

85. Nalepa M, Basheer O, Radkiewicz M, Skowrońska K, Skweres A, Owczarek A, et al. Loss of arginase 2 disrupts striatum-specific polyamine homeostasis. FEBS J. n/a. doi:10.1111/febs.70313

86. Lewis ND, Asim M, Barry DP, Singh K, de Sablet T, Boucher J-L, et al. Arginase II Restricts Host Defense to Helicobacter pylori by Attenuating Inducible Nitric Oxide Synthase Translation in Macrophages. J Immunol. 2010;184: 2572–2582. doi:10.4049/jimmunol.0902436

87. Hardbower DM, Asim M, Murray-Stewart T, Casero RA, Verriere T, Lewis ND, et al. Arginase 2 deletion leads to enhanced M1 macrophage activation and upregulated polyamine metabolism in response to Helicobacter pylori infection. Amino Acids. 2016;48: 2375–2388. doi:10.1007/s00726-016-2231-2

88. Yin Y, Phạm TL, Shin J, Shin N, Kang D-W, Lee SY, et al. Arginase 2 Deficiency Promotes Neuroinflammation and Pain Behaviors Following Nerve Injury in Mice. J Clin Med. 2020;9. doi:10.3390/jcm9020305

89. Piknova B, Park JW, Cassel KS, Gilliard CN, Schechter AN. Measuring Nitrite and Nitrate, Metabolites in the Nitric Oxide Pathway, in Biological Materials using the Chemiluminescence Method. J Vis Exp JoVE. 2016; 54879. doi:10.3791/54879

90. Hunter RA, Storm WL, Coneski PN, Schoenfisch MH. Inaccuracies of nitric oxide measurement methods in biological media. Anal Chem. 2013;85: 1957–1963. doi:10.1021/ac303787p

91. Sun J, Zhang X, Broderick M, Fein H. Measurement of Nitric Oxide Production in Biological Systems by Using Griess Reaction Assay. Sensors. 2003;3: 276–284. doi:10.3390/s30800276

92. Csonka C, Páli T, Bencsik P, Görbe A, Ferdinandy P, Csont T. Measurement of NO in biological samples. Br J Pharmacol. 2015;172: 1620–1632. doi:10.1111/bph.12832

93. Navarro LA, Wree A, Povero D, Berk MP, Eguchi A, Ghosh S, et al. Arginase 2 deficiency results in spontaneous steatohepatitis: A novel link between innate immune activation and hepatic de novo lipogenesis. J Hepatol. 2015;62: 412–420. doi:10.1016/j.jhep.2014.09.015

94. Erdely A, Kepka-Lenhart D, Salmen-Muniz R, Chapman R, Hulderman T, Kashon M, et al. Arginase Activities and Global Arginine Bioavailability in Wild-Type and ApoE-Deficient Mice: Responses to High Fat and High Cholesterol Diets. PLOS ONE. 2010;5: e15253. doi:10.1371/journal.pone.0015253

95. De Ponti FF, Liu Z, Scott CL. Understanding the complex macrophage landscape in MASLD. JHEP Rep. 2024;6: 101196. doi:10.1016/j.jhepr.2024.101196

96. Liu C, Rajapakse AG, Riedo E, Fellay B, Bernhard M-C, Montani J-P, et al. Targeting arginase-II protects mice from high-fat-diet-induced hepatic steatosis through suppression of macrophage inflammation. Sci Rep. 2016;6: 20405. doi:10.1038/srep20405

97. Tripathi A, Debelius J, Brenner DA, Karin M, Loomba R, Schnabl B, et al. The gut–liver axis and the intersection with the microbiome. Nat Rev Gastroenterol Hepatol. 2018;15: 397–411. doi:10.1038/s41575-018-0011-z

98. Wells JM, Brummer RJ, Derrien M, MacDonald TT, Troost F, Cani PD, et al. Homeostasis of the gut barrier and potential biomarkers. Am J Physiol-Gastrointest Liver Physiol. 2017;312: G171–G193. doi:10.1152/ajpgi.00048.2015

99. Ulluwishewa D, Anderson RC, McNabb WC, Moughan PJ, Wells JM, Roy NC. Regulation of Tight Junction Permeability by Intestinal Bacteria and Dietary Components1,2. J Nutr. 2011;141: 769–776. doi:10.3945/jn.110.135657

100. Balda MS, Whitney JA, Flores C, González S, Cereijido M, Matter K. Functional dissociation of paracellular permeability and transepithelial electrical resistance and disruption of the apical-basolateral intramembrane diffusion barrier by expression of a mutant tight junction membrane protein. J Cell Biol. 1996;134: 1031–1049. doi:10.1083/jcb.134.4.1031

101. Assimakopoulos SF, Tsamandas AC, Tsiaoussis GI, Karatza E, Triantos C, Vagianos CE, et al. Altered intestinal tight junctions' expression in patients with

liver cirrhosis: a pathogenetic mechanism of intestinal hyperpermeability. Eur J Clin Invest. 2012;42: 439–446. doi:10.1111/j.1365-2362.2011.02609.x

102. Assimakopoulos SF, Tsamandas AC, Tsiaoussis GI, Karatza E, Zisimopoulos D, Maroulis I, et al. Intestinal mucosal proliferation, apoptosis and oxidative stress in patients with liver cirrhosis. Ann Hepatol. 2013;12: 301–307. doi:10.1016/S1665-2681(19)31369-9

103. Scarpellini E, Valenza V, Gabrielli M, Lauritano EC, Perotti G, Merra G, et al. Intestinal Permeability in Cirrhotic Patients With and Without Spontaneous Bacterial Peritonitis: Is the Ring Closed? Off J Am Coll Gastroenterol ACG. 2010;105: 323. doi:10.1038/ajg.2009.558

104. Du Plessis J, Vanheel H, Janssen CEI, Roos L, Slavik T, Stivaktas PI, et al. Activated intestinal macrophages in patients with cirrhosis release NO and IL-6 that may disrupt intestinal barrier function. J Hepatol. 2013;58: 1125–1132. doi:10.1016/j.jhep.2013.01.038

105. Imazu N, Torisu T, Yokote A, Umeno J, Kawasaki K, Fujioka S, et al. Arginase 2 attenuates ulcerative colitis by antioxidant effects of spermidine. J Gastroenterol. 2024;59: 682–698. doi:10.1007/s00535-024-02104-z

106. Nakamura A, Matsumoto M. Role of polyamines in intestinal mucosal barrier function. Semin Immunopathol. 2025;47: 9. doi:10.1007/s00281-024-01035-4

107. Shivashankar R, Tremaine WJ, Harmsen WS, Loftus EV. Incidence and Prevalence of Crohn's Disease and Ulcerative Colitis in Olmsted County, Minnesota From 1970 Through 2010. Clin Gastroenterol Hepatol. 2017;15: 857–863. doi:10.1016/j.cgh.2016.10.039

108. P. NEJDFORS QW M EKELUND, BR WESTRÖM, O JANSSON, CL LINDSTRÖM, B KARLSSON, B JEPPSSON. Increased Colonic Permeability in Patients with Ulcerative Colitis: An in Vitro Study. Scand J Gastroenterol. 1998;33: 749–753. doi:10.1080/00365529850171701

109. HOLLANDER D, VADHEIM CM, BRETTHOLZ E, PETERSEN GM, DELAHUNTY T, ROTTER JI. Increased Intestinal Permeability in Patients with Crohn's Disease and Their Relatives. Ann Intern Med. 1986;105: 883–885. doi:10.7326/0003-4819-105-6-883

110. Pegg AE. Toxicity of polyamines and their metabolic products. Chem Res Toxicol. 2013;26: 1782–1800. doi:10.1021/tx400316s

111. Baier J, Gänsbauer M, Giessler C, Arnold H, Muske M, Schleicher U, et al. Arginase impedes the resolution of colitis by altering the microbiome and metabolome. J Clin Invest. 130: e126923. doi:10.1172/JCI126923

112. Nüse B, Mattner J. L-arginine as a novel target for clinical intervention in inflammatory bowel disease. Explor Immunol. 2021;1: 80–89. doi:10.37349/ei.2021.00008

113. Middleton SJ, Shorthouse M, Hunter JO. Increased nitric oxide synthesis in ulcerative colitis. Lancet. 1993;341: 465–466. doi:10.1016/0140-6736(93)90211-x

114. Rachmilewitz D, Stamler JS, Bachwich D, Karmeli F, Ackerman Z, Podolsky DK. Enhanced colonic nitric oxide generation and nitric oxide synthase activity in ulcerative colitis and Crohn's disease. Gut. 1995;36: 718–723. doi:10.1136/gut.36.5.718

Supplementary Information

Table 13: General lab solutions

Solution	Preparation
10x PBS • 80 g NaCl • 2 g KCl • 7.62 g Na2HPO4 • 0.77 g KH2PO4 • Distilled water	NaCl, KCl, Na2HPO4 and KH2PO4 were dissolved in 800 mL distilled water. pH was adjusted to 7.4 and the volume was brought to 1000 mL with distilled water. The solution was stored at RT.
1x PBS • 100 mL 10x PBS • 900 mL distilled water	10x PBS was added to distilled water. The solution was stored at RT.
2x PBS • 10 mL 10x PBS • 40 mL distilled water	10x PBS was added to distilled water. The solution was stored at 4 °C.

Table 14: Solutions used in the everted gut sac method

Solution	Preparation
Solution 1: 10x Salt Solution • 67.3 g/L NaCl • 3.73 g/L KCl • 1.44 g/L MgSO4 (anhydrous) • 2.22 g/L CaCl2 (anhydrous) • Distilled water	NaCl, KCl, MgSO4 and CaCl2 were dissolved in distilled water, and the volume was brought to 1000 mL. The solution was stored at 4 °C.
Solution 2: 10X HEPES Solution • 59.5 g/L HEPES • Distilled water	HEPES was dissolved in distilled water, and the volume was brought to 1000 mL. The solution was stored at 4 °C.

Solution 3: 10x KH2PO4 Solution • 1.36 g/L KH2PO4 • Distilled water	KH2PO4 was dissolved in distilled water, and the volume was brought to 1000 mL. The solution was stored at 4 °C.
KRH Buffer (100 mL): • 10 mL Solution 1 • 10 mL Solution 2 • 10 mL Solution 3 • 0.2 g BSA (0.2%) • Distilled water	The solution was prepared no longer than 48 hours before use. Solution 1, 2 and 3 were mixed, and 50 mL distilled water was added. The pH was adjusted to 7.4, and BSA was added and dissolved. The volume was brought to 100 mL with distilled water. The solution was stored at 4 °C.
Xylose Solution (0.1%) • 100 mg Xylose • 100 mL KRH Buffer	The solution was always prepared fresh before use. Xylose was dissolved in KRH Buffer.

Table 15: Solutions to assess arginase activity

Solution	Preparation
0.5 M L- Arginine • 871 mg L-Arginine • 10 mL distilled water	L-Arginine was dissolved in distilled water and pH adjusted to 9.7. The solution was stored at 4 °C.
10% Triton-X-100 • 1 mL 100% Triton-X-100 • 9 mL distilled water	100% Triton-X-100 was diluted in distilled water. The solution was stored at 4 °C.
100mM MnCl2*4H2O • 197.9 mg $MnCl_2$*$4H_2O$ • 10 mL distilled water	MnCl2*4H2O was dissolved in distilled water. The solution was stored at 4 °C.

1M Tris – HCL • 1.5 g Tris – HCL • 10 mL distilled water	Tris – HCL was dissolved in distilled water and pH adjusted to 7.4. The solution was stored at 4 °C.
Acid Mixture (1:3:7) (22 mL) • 2 mL H_2SO_4 • 6 mL H_3PO_4 • 14 mL distilled water	H_2SO_4 and H_3PO_4 were added to distilled water. Solution was stored at RT.
Alpha-ISPF • 450 mg a-ISPF • 5 mL absolute ethanol	Alpha-ISPF was dissolved in absolute ethanol. The solution was stored at 4 °C.
Lysis Buffer (6 mL) • 5490 µL Roti Water • 300 µL 100mM $MnCl_2*4H_2O$ • 150 µL 1M Tris – HCL • 30 µL Protease Inhibitor • 30 µL 10% Triton-X 100	The solution was generally prepared fresh before use. 100mM $MnCl_2*4H_2O$, 1M Tris – HCL, Protease Inhibitor and 10% Triton-X 100 were added to Roti water. Solution was stored at 4 °C and used within 1 week of preparation.
Urea Stock Solution • 80 g Urea • 10 mL distilled water	Urea was dissolved in distilled water. The solution was stored at 4 °C.

Table 16: Solutions for protein concentration determination via Bradford assay

Solution	Preparation
Color Reagent (1:5): • BioRad Protein Assay Dye Reagent Concentrate • Distilled water	BioRad Protein Assay Dye Reagent Concentrate was diluted in a ratio of 1:5 with distilled water.
Protein Standard (Stock Solution) • 100 mg BSA • 1 mL distilled water	BSA was dissolved in distilled water. The solution was aliquoted stored at -20 °C.

Table 17: Solutions for SDS-PAGE

Solution	Preparation
100 mM DTT • 30.85 mg DTT • 2 mL distilled water	DTT was dissolved in 2 mL distilled water. The solution was aliquoted and stored at -20 °C.
10x Electrophoresis Buffer • 30.28 g Tris (base) • 144.13 g Glycine • 10 g SDS • Distilled water	Tris (base), Glycine, SDS were dissolved in distilled water to an end volume of 1 L. The solution was stored at RT.
1x Electrophoresis Buffer • 100 mL 10x Electrophoresis Buffer • 900 mL distilled water	10x Electrophoresis buffer was added to distilled water. The solution was stored at RT.
4x SDS-Loading Buffer • 5.217 mL 1.5M Tris pH 6.8 • 2.5 g SDS • 12.5 mL Glycerol • 5 mL 2-B-Mercaptoethanol • 12.5 mg Bromophenol Blue • Distilled water	1.5M Tris, pH adjusted to 6.8 was mixed with SDS, Glycerol, 2-B-Mercaptoethanol and Bromophenol Blue in 25 mL distilled water. The buffer was aliquoted and stored at -20 °C.
Acrylamide (30%) • 29.2 g Acrylamide • 0.8 g N'N'-methylene-to-arylamide • 80 mL distilled water	Acrylamide and N'N'-methylene-to-arylamide were dissolved in 80 mL distilled water and filtered. The solution was stored at 4 °C.
APS (10%) • 100 mg Ammonium peri sulfate • 1 mL distilled water	APS was always prepared fresh before casting gels. APS was dissolved in distilled water.
SDS (10%) • 10 g SDS • 100 mL distilled water	SDS was dissolved in distilled water. The solution was heated up to 45 °C to dissolve if needed. The solution stored at RT.

Tris (0.5M) • 6.05 g Tris (base) • Distilled water	Tris (base) was dissolved in 90 mL of distilled water. The pH was adjusted to 6.8, and the volume was brought to 100 mL with distilled water. The solution was stored at 4 °C.
Tris (1.5M) • 18.15 g Tris (base) • Distilled water	Tris (base) was dissolved in 80 mL of distilled water. The pH was adjusted to 8.8, and the volume was brought to 100 mL with distilled water. The solution was stored at 4 °C.

Table 18: Solutions for semi-dry western blotting

Solution	Preparation
10x TBS • 48.4 g Tris (base) • 160 g NaCl • Distilled water	Tris (base) and NaCl were dissolved in distilled water. pH was adjusted to 7.6 and the volume was brought to 2000 mL with distilled water. The solution was stored at RT.
1x TBS • 100 mL 10x TBS • 900 mL distilled water	10x TBS was added to distilled water. The solution was stored at RT.
1x TBST • 100 mL 10x TBS • 900 mL distilled water • 500 µL Tween 20	10x TBS was added to distilled water. After, Tween 20 was added and dissolved. The solution was stored at RT.

Blocking Buffers • 5% Nonfat Dried Milk Powder in 1x TBST • 2.5% BSA in 1x TBST	Blocking buffers were always prepared fresh before blocking. BSA (1.25 g) or Nonfat Dried Milk (2.5 g) powder was dissolved in 1x TBST (50 mL). The blocking buffers were stored at 4 °C for a maximum of one week.
Ponceau S • 0.1 g Ponceau S • 500 µL Acetic Acid 100% • Distilled water	Ponceau S was added to acetic acid and the volume brought to 50 mL with distilled water. The solution was stored at RT.
Towbin Transfer Buffer • 3.03 g Tris (base) • 14.4 g Glycine • 200 mL Methanol • Distilled water	Tris (base) and Glycine were dissolved in Methanol, and the volume was brought to 1000 mL with distilled water. The solution was stored at RT.

Table 19: Solutions for tissue staining

Solution	Preparation
10 mM Sodium Citrate • 2.1411 g Sodium Citrate • 1000 mL distilled water	Sodium citrate was added to distilled water and pH adjusted to 6.0. Solution was stored at RT.
Blocking Buffer • 5% BSA in 1x TBST	Blocking buffer was always prepared fresh before blocking. BSA (2.5 g) was dissolved in 1x TBST (50 mL). The blocking buffers were stored at 4 °C for a maximum of one week.
DAB Chromogen Substrate Mixture • 1 mL DAB+ Substrate Buffer • 1 drop DAB+ Chromogen	The solution was always prepared fresh before use. DAB+ Chromogen was added to DAB+ Substrate Buffer.
Protease Solution • 2 mg Protease • 1 mL 1x PBS	The solution was always prepared fresh before use. Protease was dissolved in 1x PBS.